Title
CORRELATIONS BETWEEN SLOW AND FAST FRAGMENTS IN RELATIVISTIC NUCLEAR COLLISIONS

Author
Meyer, W.G.

Publication Date
1979-05-01

Lawrence Berkeley Laboratory
UNIVERSITY OF CALIFORNIA

Submitted to Physical Review C

CORRELATIONS BETWEEN SLOW AND FAST FRAGMENTS IN RELATIVISTIC NUCLEAR COLLISIONS

W. G. Meyer, H. H. Gutbrod, Ch. Lukner, and A. Sandoval

May 1979

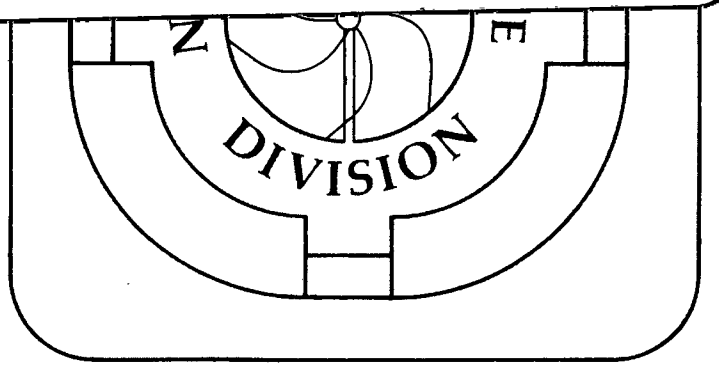

Prepared for the U.S. Department of Energy under Contract W-7405-ENG-48

DISCLAIMER

LBL-9151

CORRELATIONS BETWEEN SLOW AND FAST FRAGMENTS IN RELATIVISTIC NUCLEAR COLLISIONS

by

W. G. Meyer*, H. H. Gutbrod, Ch. Lukner
A. Sandoval

Gesellschaft für Schwerionenforschung
Darmstadt, West Germany

Lawrence Berkeley Laboratory
Berkeley, California, USA

University of Marburg
Marburg, West Germany

ABSTRACT

Heavy low energy fragments with $Z \geqslant 4$ have been measured in relativistic nuclear collisions, using a large area ionization chamber telescope. For all events, correlated slow fragments were looked for in 5 solid state counters and correlated fragments ($E > 25$ MeV/n) were measured in 80 scintillators coupled to photomultipliers. Fragment spectra were taken in the energy range of 10-150 MeV E_{total}. $p_{\parallel}$ was extracted for fission like events. Other nonbinary fragments showed an in-plane correlation with fast charged particles. Lighter particles ($4 \leqslant Z \leqslant 12$) were found to be associated with a high charged particle multiplicity. Conflicts with previous views on high energy proton-nucleus data are pointed out and a qualitative comparison to hydrodynamical effects is tried.

Nuclear Reactions:

U(p,HF) 1.05 GeV

U(p,HF), Au(p,HF) 2.1 GeV

U(^{4}He,X) Au(^{4}He,X) 400 MeV/nucleon, 1.05 GeV/nucleon

Ag(^{4}He,X) 1.05 GeV/nucleon

U(^{20}Ne,X) Au(^{20}Ne,X) Ag(^{20}Ne,X) 400 MeV/nucleon

Measured: $\sigma(E,\theta)$, associated charged particle multiplicity $M(X,\theta,\phi)$; $d^2\Omega/d\Omega_1 d\Omega_2$

X = Be to Mg, $12 < Z \leqslant 26$, $Z > 26$, Fission Fragments

PACS Index 25.70.Fg, 25.40. Rb,25.85 Ge

I. INTRODUCTION

The commonly adopted picture of a high energy proton-nucleus interaction is that of a two step process. In the first step the projectile interacts in a quasi free manner with the target nucleons producing excited target residues which, in the second step, deexcite in various possible ways, i.e., via evaporation of particles, γ-emission and fission. All the experimental studies to date[1] have led to the conclusion that the high energy proton-nucleus reaction mechanism is not fully understood.

For relativistic nuclear collisions an adoption of the two step picture seemed to be very appropriate since the apparent success of the fireball model[2] supported the separation of a fast process from a slow process as treated in the participant-spectator concept. The "slow" decay of the target spectator was calculated in various ways.[3,4] However, today several experimental results strongly challenge the validity of clean-cut participant-spectator based models, at least at Bevalac energies.[5,6,7] We want to substantiate this challenge and have developed a much more elaborate experimental setup than ever used in the previous studies. The goal was to measure spectra of slow target fragments from Be up to fission-like events, to look for coincident slow partners of similar mass, to determine the associated multiplicity of fast charged particles (known as cascade particles in the two-step model terminologies) and to look for spatial correlations between slow and fast particles. Such a spatial correlation is considered to be negligible in the framework of the above mentioned two step model and would, if

detected, be a strong indication for a collective behavior of projectile and target nucleons.

In the experimental section the details of the various counter arrangements are explained and the data-handling and -reduction is described. The associated charged particle multiplicity data is discussed, in particular the shapes of the distributions, their mean values, their spatial distributions with respect to θ and ϕ and their dependence on the trigger particle. This is followed by a section on spectra of fragments with Z values below 26. Finally the binary events are looked at and compared with data obtained at very low incident energies.

II. EXPERIMENTAL DETAILS

A. Apparatus

The apparatus used, which is schematically shown in Figure 1, consisted of three distinctively different types of equipment; (1) particle telescope, (2) silicon array, (3) plastic scintillator array. The particle telescope and silicon array were each mounted on independently moveable arms inside the one meter diameter scattering chamber. The plastic scintillator array was mounted in air outside the walls of the chamber.

The particle telescope consisted of a ΔE gas ionization chamber and three silicon surface barrier E detectors. The ionization chamber was a large volume (14.8 x 9.8 x 5.3 cm) Frisch grid chamber with an active cathode repeller plate. The chamber had a 50 $\mu g/cm^2$ polypropylene entrance window and was operated with methane gas at a pressure of 20 Torr. The three 6 cm^2 active area, 100 μm thick E detectors each had an angular resolution of $\pm 2^o$ and their centers were separated by an angle of 5.5^o. The telescope, which subtended a solid angle of 11.5 msr, was calibrated with ^{241}Am and ^{148}Gd alpha sources as well as with a ^{252}Cf spontaneous fission source.

The silicon array consisted of five 6 cm^2 active area, 100 μm thick silicon surface barrier detectors. Three of the detectors were oriented in the reaction plane as defined by the target, telescope, and beam. Each detector had an angular acceptance of $\pm 5^o$ and their centers were separated by an angle of 15^o. The array subtended a solid angle of 127.2 msr and was calibrated with ^{241}Am and ^{148}Gd sources as well as with a ^{252}Cf spontaneous fission source.

The plastic scintillator array consisted of 80 Pilot-B plastic scintillators 1/4 inch thick which were coupled to RCA 8575 photomultiplier tubes by means of lucite light pipes. Seventy-six of the scintillators were arranged in three azimuthal rings (A, B, and C) which subtended theta angles of 9^{o} to 20^{o}, 20^{o} to 45^{o}, and 45^{o} to 80^{o}, and accounted for 67% of the forward 2π. The remaining four scintillators (Ring D) were oriented in the reaction plane and subtended theta angles of 120^{o} to 160^{o} on both sides of the beam axis. The gains of the photomultiplier tubes were set with a ^{207}Bi electron source and surveyed with 80 LED's (MV 50).

A monitor telescope was used for relative normalization of each run. The monitor consisted of three 1 cm^2 Phosphorus diffused silicon detectors and was sensitive to ^{4}He ions in the energy range from 13 to 30 MeV. The monitor ΔE, E, and E_{rej} had thicknesses of 120 μm, 356 μm, and 360 μm respectively and was mounted at a theta angle of 90^{o} and a phi angle of 45^{o}.

B. Electronics

A block diagram of the electronics is shown in Figure 2. A slow coincidence between ΔE1 (anode) SCA and the E1 SCA defined a good event and served as the Master gate for the computer. A CAMAC interface was used to set bits for the three E1 and the five E2 detectors and for the pulser.

A system Busy signal was derived from an OR of the sum of the outputs of the E1 CFD's (E1 OR), the Master and the ADC Busy signal. The E1 OR was delayed a few ns and stretched to overlap the leading edge of the master and the master was stretched to overlap the leading

edge of the ADC busy signal. The E1 OR antied by the Busy signal served as the CAMAC gate. The CAMAC clear was derived from the trailing edge of the Busy.

The anode outputs of the 80 photomultiplier tubes were sent directly to 80 individual CAMAC discriminators. The width of the CAMAC gate was 50 nsec.

An E1-E2 coincidence was defined by means of a TAC. The CAMAC gate (derived from the E1 OR) was used to start the TAC and the OR of the E2 CFD's served as the stop. An SCA on the TAC output produced the E1-E2 gate and this gate was used to open the E2 LG & S.

A chopper pulser system was used to send pulser signals to all silicon detectors and the anode of the ion chamber. The pulser was externally triggered by a fraction of the monitor E_{rej} singles rate. The number of pulser events accepted by the computer served as a measure of the system dead time. The LED's of the scintillator array were triggered by an 80 output avalanche pulser which was externally triggered in the same manner as above. The LED's were only triggered every other beam burst and this allowed the determination of the accidental (trigger off) and dead time (trigger on) probabilities for the array.

C. Measurements and Data Reduction

The reactions studied are listed in Table 1. The 1 in x 2 in UF_4, Au, and Ag targets used had thicknesses of 699, 1030, and 647 $\mu g/cm^2$ respectively. The Ag target was self-supporting and the UF_4 and the Au targets were prepared by vacuum evaporation onto 50 $\mu g/cm^2$ polypropylene foils.

The information obtained in this experiment was four-fold.

1. $d^2\sigma/dEd\Omega$ as a function of laboratory angle
2. $d^2\sigma/d\Omega_1 d\Omega_2$ as a function of coincidence angle
3. Associated charged particle multiplicity
4. Azimuthal correlations

The $d^2\sigma/dEd\Omega$ information was obtained, as a function of the Z of the reaction product, with the particle telescope. Figure 3 shows a schematic ΔE vs E contour, and the lines indicate the software windows used to divide the data into eleven groups as a function of Z. The telescope yielded individual Z resolution which could be followed up to a Z of 26. However, due to poor statistics, the data with $13 \leqslant Z \leqslant 26$ were grouped together. The $d^2\sigma/dEd\Omega$ for $4 \leqslant Z \leqslant 12$ were corrected for one-half the target thickness as seen by the telescope at each laboratory angle. In all cases, this correction was less than the energy bin size used in the data reduction. The absolute normalization of the data was determined from knowledge of the telescope solid angle, target thickness and absolute beam flux. The absolute beam flux was measured with an Ar filled gas ionization chamber which was calibrated by the direct counting of beam particles as described in Ref. 6.

The $d^2\sigma/d\Omega_1 d\Omega_2$ information was obtained from coincidence measurements between the particle telescope and the silicon array. The particle telescope was sensitive to fragments with $Z > 4$ and total energies $E \geqslant 5$ MeV. The silicon array was sensitive to any particle that would deposit 6 MeV or more in a 100 μm thick silicon detector, for example, the array was sensitive to alpha particles in the energy range of

6 to 20 MeV. For true binary events, as in the case of statistical fission, the $d^2\sigma/d\Omega_1 d\Omega_2$ information was used to extract a value of the most probable linear momentum transferred to the fissioning nucleus. This information was obtained by means of an iterative process utilizing the total energy of both fragments, the coincidence angle between them, and a guess of the fissioning nucleus which was based upon the measured charge particle multiplicity. However, for a coincidence between $4 \leqslant Z \leqslant 26$ in the particle telescope and something in the silicon array, the $d^2\sigma/d\Omega_1 d\Omega_2$ was only useful in determining whether or not there was evidence of a two body correlation.

The associated charged particle multiplicy information was obtained by measuring the number of fast charged particles that triggered the scintillator array in coincidence with observing a particular fragment in the particle telescope. The low energy thresholds for observing particular charged particles in the plastic scintillators are given in Table 2. One quantitative piece of information that can be extracted from these measurements is the average real associated charge particle multiplicity. This average multiplicity was determined by adopting the standard techniques developed for γ-ray multiplicity measurements,[8] correcting for missing solid angle, coincidence summing, and accidental and dead time probabilities, assuming uniform azimuthal distributions and no correlations in particle emission. This procedure was applied to the multiplicity information in each of the four rings yielding a quantity $d\langle m\rangle/d\Omega(\theta)$. The average real multiplicity was determined

by integrating $d\langle m\rangle/d\Omega(\theta)$ from 0 to π. The accidental and deadtime probabilities were small, of the order of a few percent, in all cases.

The final piece of information obtained from this experiment concerns azimuthal correlations ($d^2\sigma/d\Omega_1 d\Omega_2(\theta)$, where $\phi = |\phi_1 - \phi_2|$) between slow fragments detected in the particle telescope and fast particles detected in the plastic scintillator array. In order to determine if such a correlation exists, a two particle correlation function was extracted from the data. In particular, the R function[9] which is defined as

$$R = \sigma_R \frac{\dfrac{d^2\sigma}{d\Omega_1 d\Omega_2}}{\dfrac{d\sigma_1}{d\Omega_1}\dfrac{d\sigma_2}{d\Omega_2}} - 1$$

was used, where σ_R is the total inelastic cross-section and $d\sigma_1/d\Omega_1$ and $d\sigma_2/d\Omega_2$ are the single particle inclusive cross-sections for particle 1 and 2 respectively. The advantage of R is that it measures the fractional correlation and therefore treats favoured and unfavoured regions of phase space equally.

III. DISCUSSION

A. Associated Charged Particle Multiplicities

1. Shapes of Multiplicity Distributions

The slope of the observed associated charged particle multiplicty distribution, as measured in the 80 counter multiplicity array previously described, can provide insight into the type of interaction that produced the trigger particle. For example, if the trigger particle was associated predominantly with a large multiplicity of fast charged particles, it would be assumed to come from a central collision, and low associated multiplicity would imply a rather peripheral collision.

Figure 4 shows six distinctively different associated charge particle multiplicity distributions from interactions of ^{20}Ne and ^{4}He projectiles with targets of Au and U. The left hand portion of Figure 4 shows the distributions associated with protons and carbon ions. The distribution associated with observing a proton ($25 \leq E \leq 200$ MeV) at a laboratory angle of 90^{o} shows a significant amount of low as well as high multiplicity events, indicating that protons are produced in both violent (central) and gentle (peripheral) interactions. In contrast to this, the distribution associated with seeing a low energy carbon ($5 \leq E \leq 140$ MeV) at 90^{o} in the laboratory is characterized by an absence of zero multiplicity, i.e. a distribution almost symmetric about the most probable value. This shape and the magnitude of the multiplicity, indicate that low energy, light fragments ($4 \leq Z \leq 12$) come almost exclusively from central collisions and are not produced in peripheral collisions. High energy proton, heavy emulsion nuclei studies,[10,11] have also shown that light fragments, in particular ^{8}Li

and ^{8}B are predominantly produced in interactions with the largest number of charged particle prongs, i.e. the most violent proton nucleus reactions.

The central portion of Figure 4 compares observed multiplicity distributions associated with fragments with $Z > 26$ from interactions of ^{20}Ne with targets of U and Au. The distribution from the U target exhibits a maximum probability near zero multiplicity, with almost no high multiplicity events. The distribution from the Au target has two components, a low and a high multiplicity component. The difference in the multiplicity distributions reflect the difference of the nuclear properties of the two target nuclei. In the case of the U target, which has a low fission barrier, approximately 90% of the fragments with $Z > 26$ are produced by means of a statistical fission process. On the other hand, less than 10% of the fragments with $Z > 26$ come from a statistical fission process in the case of the Au target, which has a much higher fission barrier than U. The nature of the U distribution indicates that these fission events are produced almost entirely in peripheral interactions with small energy and momentum transfer.

In order to further investigate the two component distribution associated with fragments with $Z > 26$ from a Au target we can look at the multiplicity distributions associated with all $Z > 26$ events measured and the distribution associated with observing two slow moving fragments in coincidence. As can be seen in the right hand portion of Figure 4, if a binary slow fragment event is selected, the low multiplicity component is enhanced. However, the high multiplicity

component is still present. The presence of the high multiplicity component, associated with two slow moving fragments, may be an indication of a new reaction mechanism. A mechanism where by the projectile knocks out a reasonable amount of the target nucleus and leaves two rather cold (i.e. low excitation energy) pieces which are driven apart, without forming a long neck, by their Coulomb forces. A similar mechanism has been postulated to explain some recent high-energy-proton nucleus data.[12]

2. Angular Distributions of Average Multiplicities

The manner in which the fast charged particles, associated with a given trigger particle, are distributed over 4π can give qualitative information concerning the nature of the interaction between the projectile and the target. For example, if the laboratory distribution of fast charged particles is strongly forward peaked, this is an indication of interactions involving very small amounts of transverse momentum transfer, such as in the case of projectile fragmentation. Therefore, the flatter the laboratory distribution, the larger the transverse momentum transfer, i.e. a larger fraction of the initial longitudinal momentum of the projectile is being damped into transverse degrees of freedom.

With our multiplicity array, we can look at the average number of particles, associated with a given trigger particle, that populate four regions of 4π. Figure 5 shows three different laboratory angular distributions of average associated multiplicities, $d\langle M\rangle/d\Omega$. As can be seen in Figure 5, the distribution associated with observing coplanar binary fission events is extremely forward peaked. In contrast, the

angular distributions associated with observing protons ($25 \leq E \leq 200$ MeV) are much flatter, with the distribution associated with observing an oxygen being the least forward peaked. This information complements what we learned from the shapes of the associated charged particle multiplicity distributions. Namely, fission fragments (as from a statistical fission process) are produced in relatively gentle, peripheral collisions and low energy light fragments ($4 \leq Z \leq 12$) are produced in rather violent central collisions.

These angular distributions of average associated multiplicities, associated with a) fission products, b) protons, and c) light fragments (Figure 5) show that in going from a) peripheral collisions to b) near central collisions to c) predominantly central collisions, the transverse particle flux increases.

3. Mean Associated Multiplicities

The integrated area under the curves shown in Figure 5, yields the real mean associated charged particle multiplicity associated with a given trigger particle. The results of such integrations are plotted in Figure 6 as a function of the Z of the trigger particle. One can see from Figure 6 that fragments with $4 \leq Z \leq 12$ have the highest real mean multiplicity and that for a given projectile and energy, the multiplicity scales with the mass of the target nucleus.

Figure 7 shows a new and very interesting phenomena: for a given target nucleus, the real mean associated charged particle multiplicity scales with the total energy of the projectile, not with the projectile velocity. This new information indicates for the first time that the total energy brought in by the projectile is an important variable

to look at in trying to understand the mechanisms involved in relativistic nuclear collisions.

The scaling of the multiplicity with the total energy of the projectile does not tell the entire story as can be seen in Figure 8. There, a comparison is made of $d\langle M\rangle/d\Omega$ for ^{4}He + Au and ^{20}Ne + Au where the projectile energy is approximately the same, namely 8 GeV. One sees that the angular distribution for the 400 MeV/n ^{20}Ne + Au reaction is slightly more forward peaked than for the 2100 MeV/n ^{4}He + Au reaction. This observation indicates a kinematical effect that is associated with the total incoming momentum, rather than the momentum per nucleon of the projectile.

B. Azimuthal Correlations

Figure 9 shows several two particle correlation functions between slow moving light and heavy fragments detected at $\phi = 0^{o}$ and $\theta = 90^{o}$ in the detector telescope and fast moving ($E \geq 25$ MeV/n) charged particles detected in Rings A and B of the multiplicity array. If one compares the three lower frames of Figure 9 (400 MeV/n ^{20}Ne + Au) one can see an increasing enhancement in the correlation function at $\phi = 180^{o}$ as the Z of the correlated slow fragment increases. That is, the correlation functions between Z = 6 and fast charged particles is nearly isotropic, where as for fragments with Z > 26 (from a Au target) there is approximately a factor of two enhancement in the correlation at $\phi = 180^{o}$ in both Rings A and B.

The top frame of Figure 9 shows the correlation functions for 400 MeV/n ^{20}Ne + U $\rightarrow$ Z = 26 + X. It can be seen that unlike the Au target, there are no statistically significant correlations between

fast charged particles and $Z > 26$ fragments for the U target. This lack of correlation can be understood by recalling that a) the smallest theta angle covered by the multiplicity array is $\theta = 9^o$ and b) that 90% of yield in the $Z > 26$ group from a U target comes from a statistical fission process, which at these bombarding energies, are predominantly a result of a gentle, peripheral interaction as shown by their multiplicity distributions. One might expect to see some asymmetry in the phi distributions of correlated fast charged particles in regions of theta less than 9^o, since projectile fragmentation studies[13] have shown that there are small amounts of perpendicular momentum transferred in such interactions.

The phi-symmetry of the fast charged particles that are correlated with slow moving fragments with $4 \leqslant Z \leqslant 12$ and the phi-asymmetry associated with $Z \geqslant 26$ fragments (from targets such as Ag and Au) can be seen in Figure 10. This figure shows two typical events as measured by the multiplicity array in coincidence with an oxygen fragment (upper half) and a $Z = 26$ fragment (lower half).

The lower half of Figure 10 is especially interesting since the momentum of the $Z = 26$ fragment is approximately 2 GeV/c, (since the $Z = 26$ fragment is detected at a laboratory angle of 90^o, this momentum is essentially the perpendicular momentum of the fragment). With a projectile velocity of 400 MeV/n, it is impossible to transfer this amount of momentum ($p_\perp = 2$ GeV/c) perpendicular to the beam direction in a single nucleon-nucleus collision. Therefore, such events (lower half of Figure 10), indicate a cooperative interaction mechanism between many nucleons of the projectile and the target.

This observed asymmetry obviously indicates conservation of momentum, and since the momenta are smaller for the light fragments, the asymmetry may also be smaller. However, remember an in-plane correlation between a large number of fast charged particles and one heavy intact nucleus is observed. The mechanism for this observed momentum balance, coupled with small excitation of a substantial portion of the target is very intriguing and worth understanding. First results of hydrodynamical calculations[5,14,17] look very encouraging, since they predict for nonzero impact parameter collisions an in-plane 180° correlation between fast fragments and very slow ones with velocities close to our measured ones of 0.07 c to 0.04 c (Fig. 11).

C. Fragment Spectra

In high energy-proton nucleus reactions low energy fragments from targets like uranium exhibit the following features:[1] a) there are peaks in the spectra which shift towards higher energy as the atomic numbers of the fragments increase. They are interpreted in a simple two step model as a reflexion of the Coulomb barrier at the emission point. b) this apparent Coulomb barrier is one half or less of the nominal Coulomb barrier of the composite system (moving with a given $\beta_{\parallel}$ and $\beta_{\perp} = 0$). c) the slope of the spectra at 90° reflects, in the above mentioned two step model, the temperature of the emitting source and values as high as 10 to 30 MeV have been reported.

Later studies[15] with incident deuterons and alpha-particles showed a further decrease of the apparent Coulomb-barrier and an increase in the apparent temperature. It was pointed out that the complex

particles apparently deposited more energy in the target nucleus than did the protons.

Finally in these studies[1,15] it was pointed out that all the data were more forward peaked in intensity than could be explained by this simple model of a forward moving source of a certain temperature emitting fragments isotropically in its rest frame.

In this experiment these low energy fragments were found to be associated with high multiplicities, substantiating the earlier conclusions (Sec. A.1) that these fragments indeed come from very violent reactions, where large amounts of energy is dissipated in the target nucleus. Figure 12 shows the 90^{o}-spectra of fragments of Z = 6 to Z = 11 from 1.05 GeV/n ^{4}He on Au. As in high energy proton-nucleus reactions the peak energy shifts towards higher values with increasing atomic number. As the incident energy is increased, as shown in Fig. 13, the peak position for carbon fragments is shifted to a lower energy by approximately 6 MeV. Since we measured in this experiment the associated charged particle multiplicity we find in the comparison that for carbon produced by the interaction of 8.4 GeV ^{4}He + U there on the average 22 fast charged particles observed whereas for 4.2 GeV ^{4}He + U, carbon fragments are associated with only 13 fast charged particles. Therefore, at 8.4 GeV incident ^{4}He on U the remaining system has on the average <u>at least</u> 9 charges less than at 4.2 GeV and thus has a lower effective Coulomb barrier. A look at the slope of the spectra indicates a flatter spectra at the higher energy, corresponding to an "apparent higher temperature" of the excited nuclear system.

Since a lower limit of the amount of charge removed from the composite system has been measured in this experiment, one can try to see whether this explains the apparent reduction of the Coulomb barrier in the emission of light fragments. Using the peak energies of carbon and neon fragments and the slope of the spectra for the apparent temperatures and assuming that the emitting source is the same for carbon or neon emission then the apparent second body in the carbon emission at 8.4 GeV has an atomic number of about 42 and a reduced Coulomb radius of r_0 = 2.0 fm. This is low compared to the upper limit of 65 which is the sum of $Z_{projectile} + Z_{target} - Z_{carbon} - \langle M \rangle$. Part of that difference may be explained by the missing particles with energies below 25 MeV/n, part may be due to doubly charged clusters of energy larger than 25 MeV/n. The large apparent Coulomb radius for a Z = 42 nuclear system, however, indicates a very high deformation of the emitting system.

The second body was looked for in the coincidence detectors which has a lower threshold of 6 MeV. Because of this threshold and pulse height defect of the detectors we were not able to measure the coincident fragment (if any existed) from the U target, since the heavy coincident particle would produce a signal below this threshold. For the Ag-target, however, there are lighter m_2 masses involved yielding higher recoil velocities, but we observed no correlation between light fragments in the ionization chamber telescope and the coincidence counters. Figure 14 shows the carbon - anything above 6 MeV correlation from 187° to 116°. Compare its flat shape with that of binary fission-like fragments shown in Figure 19.

In Figure 15 the double differential cross section is increasing with decreasing emission angle. This enhancement is usually described as being due to the forward motion of the isotropically emitting hot source and forward velocities in the vicinity of 0.04c - 0.06c have been extracted.

Since the light fragments discussed here are ear marked by their high associated charged particle multiplicity to come predominantly from central collisions, those findings together with the indicator of large deformation effects suggest that one should drop the simple two step model in these reactions and turn to models with more complex dynamics in the emitting systems. Whereas the cascade model predicts residues to recoil into finite angles,[16] hydrodynamical calculations, on the other hand, predict that for central collisions a nuclear system expands, strongly oriented with respect to the incident path of the projectile, causing a polarization of the exploding system.[14,17,18] (Fig. 11, 16). In the latter case it can easily be seen, that large differences in Coulomb repulsion occur for clusters frozen out at different polar angles. Thus an extraction of a parallel velocity is very difficult because of the strongly varying Coulomb force as a function of polar angle.

In this context we would like to point out once more, that there is a large amount of high energy proton-nucleus data which could never be fully explained consistently at all angles, since the data were always more forward peaked.

D. Fission

Sample fission fragment kinetic energy spectra from the fission of U induced by projectiles of ^{4}He and ^{20}Ne are presented in Figure 17. As can be seen, the spectra are symmetric in shape. This symmetry is characteristic of a fissioning nucleus with an excitation energy, $E^* \geqslant 50$ MeV.[19]

The right half of Figure 17 shows fission kinetic energy spectra at laboratory angles of 90^{o} and 30^{o}. The increase in yield between 90^{o} and 30^{o} is consistant with a $1/\sin\theta$ shape, indicating that some amount of angular momentum has been imparted to the fissioning nucleus. A more quantitative analysis of this anisotropy allows one to estimate a lower limit of angular momentum.[19] Since, a complete fission fragment angular distribution was not measured, we can not extract from the data the mean amount of angular momentum, imparted to the fissioning nucleus. However, we can obtain an estimate of $\langle \ell \rangle$ by comparing the measured fission fragment anisotropy ratio, $d\sigma/d\Omega\,(30^{o})/d\sigma/d\Omega\,(90^{o}) = 1.31$, for the 400 MeV/n ^{20}Ne + U reaction with anisotropies measured[20] for ^{4}He + U at projectile energies between 7 to 35 MeV/n where values of $\langle \ell \rangle$ are reasonably well known. The anisotropy of 1.31 agrees with the anisotropy measured[20] for 11 MeV/n ^{4}He + U. Since the value of $\langle \ell \rangle$ is 13 for 11 MeV/n ^{4}He + U ($\langle \ell \rangle = 2/3\ \ell_{max}$), we can conclude that the average amount of angular momentum imparted to the fissioning nucleus by the interaction of a 400 MeV/n ^{20}Ne projectile with a U target is at least $13\hbar$. This value is in the vicinity of an angular momentum value of $18\hbar$ extracted from knowledge of the linear momentum transferred to the fissioning system (Table 4) assuming a large

impact parameter of a peripheral reaction. This value is small compared to a $\langle \ell \rangle \simeq 420\hbar$ which is allowed for the 400 MeV/n ^{20}Ne + U reaction, indicating that interactions which lead to fission of the target nucleus are rather gentle. However, the fact that an angular momentum of $13\hbar$ is transferred does indicate that fission is induced in reactions with a reasonable amount of projectile-target interaction.

The cross sections for fission, σ_f, determined in this work, are listed in Table 3 along with calculated[21] values of σ_R. The values of σ_f for ^{4}He + U at projectile energies of 400, 1050, and 2100 MeV/n are compared with measured σ_f values between 7 and 35 MeV/n,[20,22] in Figure 18. As can be seen, there is a decrease in σ_f of more than a factor of two between 35 MeV/n and 2100 MeV/n. Also shown in Figure 18 are measured[20,22] (18 and 35 MeV/n) and calculated (400, 1050, and 2100 MeV/n) values of the total inelastic cross section, σ_R. It can be seen that at 35 MeV/n and below $\sigma_f = \sigma_R$ (Ref. 22) and that above 400 MeV/n σ_R appears to be constant and roughly equivalent with the value at 35 MeV/n. It is interesting to note that, even though σ_R is constant, σ_f is decreasing rather rapidly between 400 and 2100 MeV/n. This divergence between σ_R and σ_f shows, that as the projectile energy is increased, a larger fraction of the projectile-target interactions are violent. That is, larger amounts of energy are deposited in the target making it impossible for the target to undergo equilibration followed by a statistical fission decay.

A sample fission fragment correlation function is shown in Figure 19. If there was no linear momentum transferred to the fissioning nucleus, a narrow peak would be observed (whose width and shape would be determined

by the number of neutrons that were evaporated from the fission fragments) centered at a $\Delta\theta = 180^{o}$. As can be seen in Figure 19, the correlation function is peaked at a $\Delta\theta$ slightly less than 180^{o}, indicating that some linear momentum was transferred to the fissioning nucleus. It is of interest to note that the correlation function is skewed toward decreasing values of $\Delta\theta$, showing that some fraction of the fissioning nuclei receive rather substantial amounts of linear momentum.

The fission-fission correlation data was used to extract a most probable value of the linear momentum ($p_{\parallel}$) transferred to the fissioning nucleus, utilizing the procedure outlined in section II.C. The results of this calculation are tabulated in Table 4. As can be seen, the values of $p_{\parallel}$ range from 220 to 500 MeV/c. To put these values in the proper perspective, studies[13] have shown that $p_{\parallel}$ transferred in projectile fragmentation reactions are of the order of 100 MeV/c. Therefore, the interactions leading to fission can be considered slightly more violent than interactions that lead to the low excitation energy break-up of the projectile.

IV. CONCLUSION

From the shapes of the associated charged particle multiplicity distributions it became evident that - as expected - fission fragments from relativistic nuclear collisions are predominantly produced in low multiplicity events. However, a component with high multiplicities has been found, indicating that even in violent reactions binary fragments are produced, possibly via an interesting new mechanism.

The low-Z fragments are originating from events with high multiplicity as was expected from earlier high energy proton-nucleus data. However the strong lack of low multiplicity events contributing to this channel is a surprising result and makes these low Z fragments, in the absence of multiplicity counters, an excellent indicator of a very violent collision.

The puzzling apparent reduction of the Coulomb barrier for emitted light fragments from heavy target nuclei bombarded by high energy protons is also observed here in relativistic nuclear collisions with heavy target-nuclei. However it was found that the apparent Coulomb barrier decreases as the total incident kinetic energy increases. Furthermore, it could be shown by measuring simultaneously the associated charged particle multiplicity of fast particles ($E \geqslant 25$ MeV/n) that apparent Coulomb barrier (peak position in the spectra), apparent temperature (inverse slope of the spectra) and the average charged particle multiplicity are all related to the incident total kinetic energy. For heavier fragments of nonbinary nature a strong 180^{o} in plane correlation was found with many fast particles. This in-plane-180^{o} correlation between slow and fast particles strongly questions

the old two-step picture for a high-energy projectile-nucleus interaction and definitely links the fast particles to the bulk motion of the target remains. The one fluid hydrodynamical models invite one to understand all these many features. For central collisions these calculations predict strong absorbtion of the total kinetic energy by the target nucleus and, further, an expansion leading to shapes that appear to account for the Coulomb effects observed. In violent peripheral reactions the calculations agree with the velocities observed for the heavy particles and with their in-plane-180^{o} correlation with fast charged particles.

The fission cross section from Uranium decreases rapidly as the bombarding energy increases. At low energies 35 MeV/n, the Uranium nucleus had essentially 100% chance to undergo fission even for central collisions.[22] As the projectile energy increases the collisions get more and more violent, and only in more peripheral collisions is the excitation low enough for a statistical fission process to occur. However, as the studies with a Au target have shown, there is a binary fragmentation process associated with violent collisions.

ACKNOWLEDGMENTS

This work was supported by the Bundesministerium für Forschung und Technologie, West Germany and in part by the Nuclear Physics Division of the U.S. Department of Energy under contract no. W-7405-ENG-48.

In particular we would like to acknowledge the support of the Zentrale Technik and the Mechanik Werkstatt at GSI in the construction of the ion chamber telescope and the help of R. J. Force and the Bevalac crew during the experiments. We are grateful for stimulating discussions with Drs. H. Stöcker, C. Y. Wong, Y. Yariv and Z. Fraenkel.

REFERENCES

*Present address: Bell Laboratories, Reading, Pennsylvania 19604

1. G. D. Westfall, R. G. Sextro, A. M. Poskanzer, A. M. Zebelman, G. W. Butler, and E. K. Hyde, Phys. Rev. C17, 1368 (1978) and references therein.
2. J. Gosset, H. H. Gutbrod, W. G. Meyer, A. M. Poskanzer, A. Sandoval, R. Stock, and G. D. Westfall, Phys. Rev. C16, 629 (1977).
3. W. Loveland, R. J. Otto, D. J. Morrissey and G. T. Seaborg, Phys. Lett. B 69, 284 (1977).
4. B. Grammaticos and A. Lumbroso CEN Saclay, Report DPh-T/79/36, March 1979.
5. H. H. Gutbrod, Proceedings of 4th Summerstudy of Relativistic Nuclear Collisions, July 1978, LBL-7766, p. 1.
6. A. Sandoval, H. H. Gutbrod, W. G. Meyer, A. M. Poskanzer, R. Stock, J. Gosset, J.-C. Jourdain, C. H. King, G. King, Ch. Lukner, Nguyen Van Sen, G. D. Westfall, and K. L. Wolf, preprint (1979) LBL-7766, submitted for publication.
7. R. Stock, H. H. Gutbrod, W. G. Meyer, A. M. Poskanzer, A. Sandoval, J. Gosset, Ch. King, G. King, Ch. Lukner, N. Van Sen, G. D. Westfall, K. L. Wolf, to be published, and S. Nagamija, Proceedings of 4th Summerstudy of Relativistic Nuclear Collisions, July 1978, LBL-7766, p. 71.
8. G. B. Hagemann, R. Broda, B. Herskind, M. Ishihara, S. Ogaza, and H. Ryde, Nucl. Phys. A 245, 166 (1975).
9. J. D. Jackson in Phenomenology of Particles at High Energies, R. L. Crawford and R. Jennings, Eds. (Academic Press, London, 1974) p. 97.

10. R. Kaczarowski, E. Makowska, Nucl. Phys., 74 (1965) p. 348.

11. W. Gajewski, J. Pnieski, J. Sieminska, J. Suchorzewska, P. Zielinski, Nucl. Phys. 58 (1964) 17.

12. B. D. Wilkins, S. B. Kaufman, E. P. Steinberg, J. A. Urbon, D. J. Henderson, submitted to Phys. Rev. Letters, August 1979.

13. D. E. Greiner, P. J. Lindstrom, H. H. Heckman, B. Cork, F. S. Bieser, Phys. Rev. Lett. 35, 152 (1975).

14. A. A. Amsden, J. N. Ginocchio, F. H. Harlow, J. R. Nix, M. Danos, E. C. Halbert, and R. K. Smith, Jr., Phys. Rev. Letters 38, 1055 (1977).

15. A. M. Zebelman, A. M. Poskanzer, J. D. Bowman, R. G. Sextro, V. E. Viola, Phys. Rev. C 11 (1975) p. 1280.

16. Y. Yariv and Z. Fraenkel, Rehovot, preprint 1979 WIS-79/15-Ph and private communications.

17. H. Stöcker, J. A. Maruhn, and Z. Greiner, Z. F. Physik , in print.

18. H. H. K. Tang and C. Y. Wong, to be published and private communications.

19. R. Vandenbosch and J. Huizenga, Nuclear Fission (Academic Press, New York, 1973).

20. W. G. Meyer, Ph.D. Dissertation, University of Maryland, 1975.

21. P. J. Karol, Phys. Rev. C 11, 1203 (1975).

22. W. G. Meyer, V. E. Viola, R. G. Clark, R. B. Theus, to be published in Phys. Rev. C. November, 1978.

Table 1. Table of Reactions Studied.

Projectile	Energy (GeV/n)	Target	Reaction Product*
P	1.05	U	HF
	2.1	U, Au	HF
^{4}He	0.400	U, Au	Z=4 to HF
	1.05	U, Au	Z=4 to HF
	2.1	U, Au, Ag	Z=4 to HF
^{20}Ne	0.400	U, Au, Ag	Z=4 to HF

*HF refers to products with $Z \geq 26$ and fission fragments. The energy of the products was $E \geq 5$ MeV.

Table 2. Thresholds for Charged Particles in the Scintillator Array.

Particle	Energies
π^{+}	10 MeV
P	25 MeV/n
d	17 MeV/n
t	13 MeV/n
^{3}He	29 MeV/n
^{4}He	25 MeV/n

Table 3. Fission and total inelastic cross sections.

Reaction	σ_f(mb)	σ_R(mb)[a]
400 MeV/n ^{4}He + U	1460 ± 140	2330
1050 MeV/n ^{4}He + U	1050 ± 100	2500
2100 MeV/n ^{4}He + U	920 ± 90	2500
400 MeV/n ^{20}Ne + U	1620 ± 160	4100

[a]Calculated using soft sphere model of Ref. 21.

Table 4. Most probable values of $p_{\parallel}$.

Reaction	$p_{\parallel}$ (MeV/c)
400 MeV/n ^{20}Ne + U	500
400 MeV/n ^{4}He + U	480
1050 MeV/n ^{4}He + U	430
2100 MeV/n ^{4}He + U	220

FIGURE CAPTIONS

Figure 1. Schematic of experimental configuration, showing multiplicity array, ion-chamber-Si telescope and Si array.

Figure 2. Block diagram of electronic configuration. PA = Pre-amplifier, CFD = Constant Fraction Discriminator, LA = Linear Amplifier, TAC = Time-to-Amplitude Converter, and LG&S = Linear Gate and Stretcher.

Figure 3. Schematic E versus E two dimensional contour. The solid lines indicate the software windows used in the data analysis.

Figure 4. Observed associated charged particle multiplicity distribution, as measured with the 80 counter multiplicity array, plotted as a probability.

Figure 5. Angular distribution of associated charged particle multiplicities.

Figure 6. Real mean associated charged particle multiplicities plotted as a function of the Z of the trigger particle for 400 MeV/n ^{20}Ne projectiles interacting with targets of Au and Ag.

Figure 7. Real mean associated charged particle multiplicities plotted as a function of the Z of the trigger particle.

Figure 8. Angular distribution of associated charged particle multiplicities.

Figure 9. Azimuthal correlations between fast charged particles and slow moving fragments.

Figure 10. Sample multiplicity patterns as detected in the 80 counter array in coincidence with an oxygen fragment (upper half) and a Z = 26 fragment (lower half).

Figure 11. Hydrodynamical calculations for Ne + U at 400 MeV/n from Ref. 17 showing the bounce-off effect which leads to a spray of fast particles in a 180^{o} in-plane correlation to the target remains recoiling with velocities up to 0.07c.

Figure 12. Laboratory kinetic energy spectra, taken at $\theta_{lab} = 90^{o}$, for $6 \leqslant Z \leqslant 11$.

Figure 13. Laboratory kinetic energy spectra for carbon ions at $\theta_{lab} = 90^{o}$ for the interaction of 1050 and 2100 MeV/n ^{4}He + Au.

Figure 14. Carbon-heavy/light fragment two particle correlation function.

Figure 15. Laboratory kinetic energy spectra for carbon ions at three laboratory angles.

Figure 16. Hydrodynamical calculations of a central collision of 400 MeV/n ^{20}Ne on U (Ref. 17). Fragments are emitted with the local expansion velocity with an additional acceleration by the local Coulomb force which is different at different polar angles.

Figure 17. Laboratory fission fragment kinetic energy spectra.

Figure 18. Cross sections for fission, σ_f, and total inelastic cross sections, σ_R, for the interaction of ^{4}He + U:
■ : σ_f this work, □ : σ_R, calculated using model of Ref. 22, ● = σ_f from Ref. 21, Δ = σ_R from Ref. 21.

Figure 19. Fission-fragment fission-fragment angular correlation function.

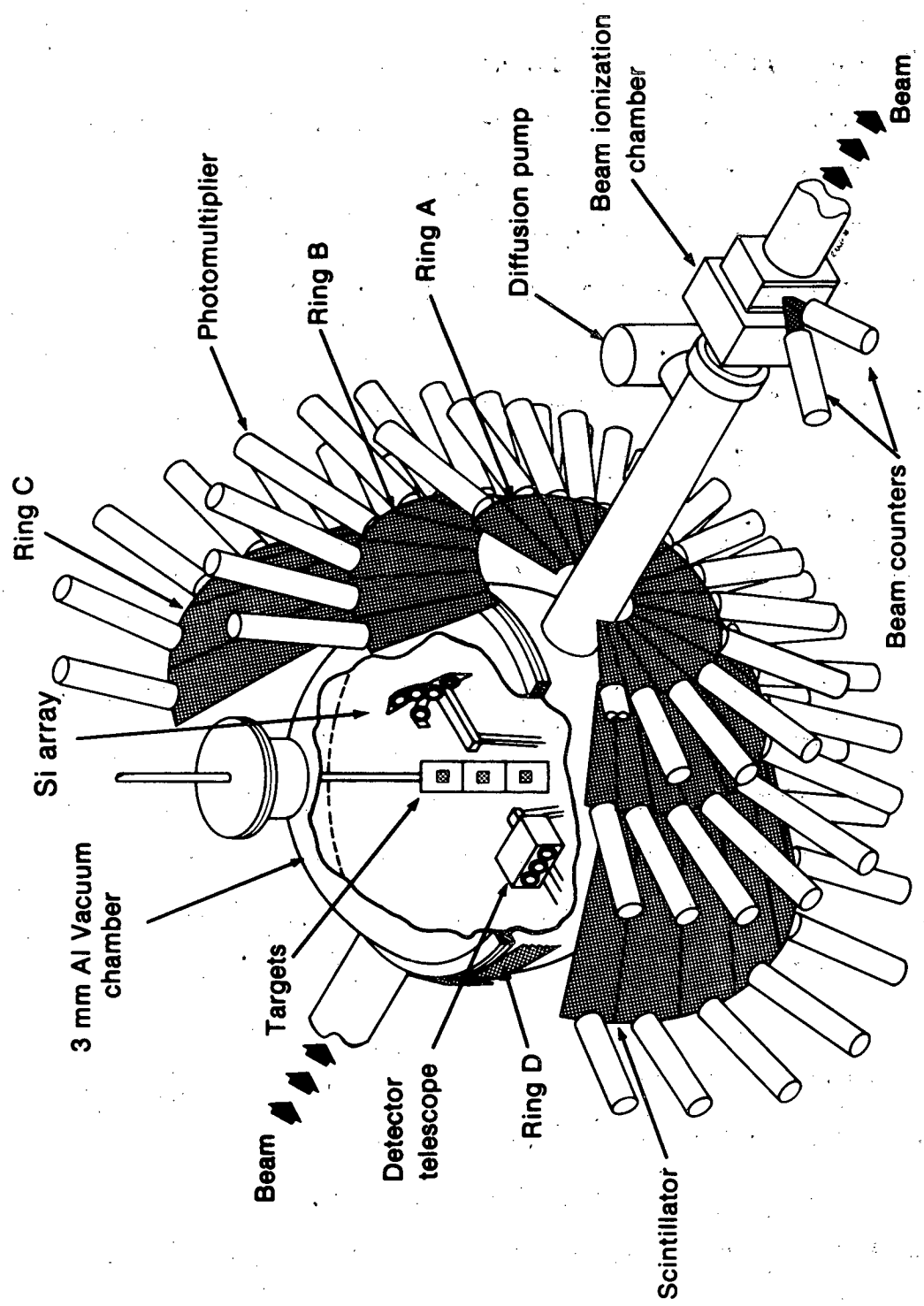
Ring C
Photomultiplier
Ring B
Ring A
Diffusion pump
Beam ionization chamber
Beam
Si array
3 mm Al Vacuum chamber
Targets
Beam counters
Detector telescope
Ring D
Scintillator
XBL 794-1097

Figure 1

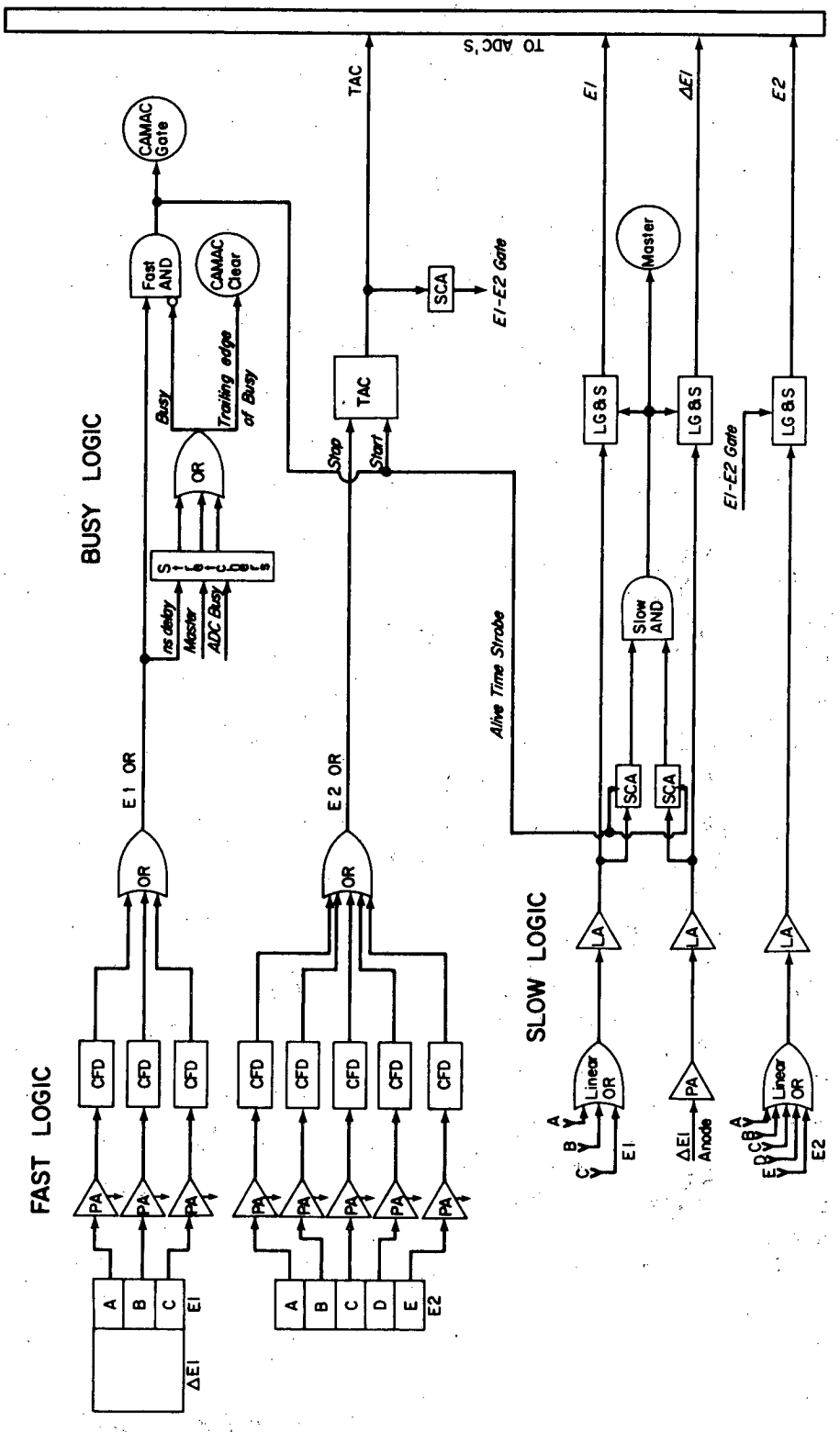

XBL 794-1098

Figure 2

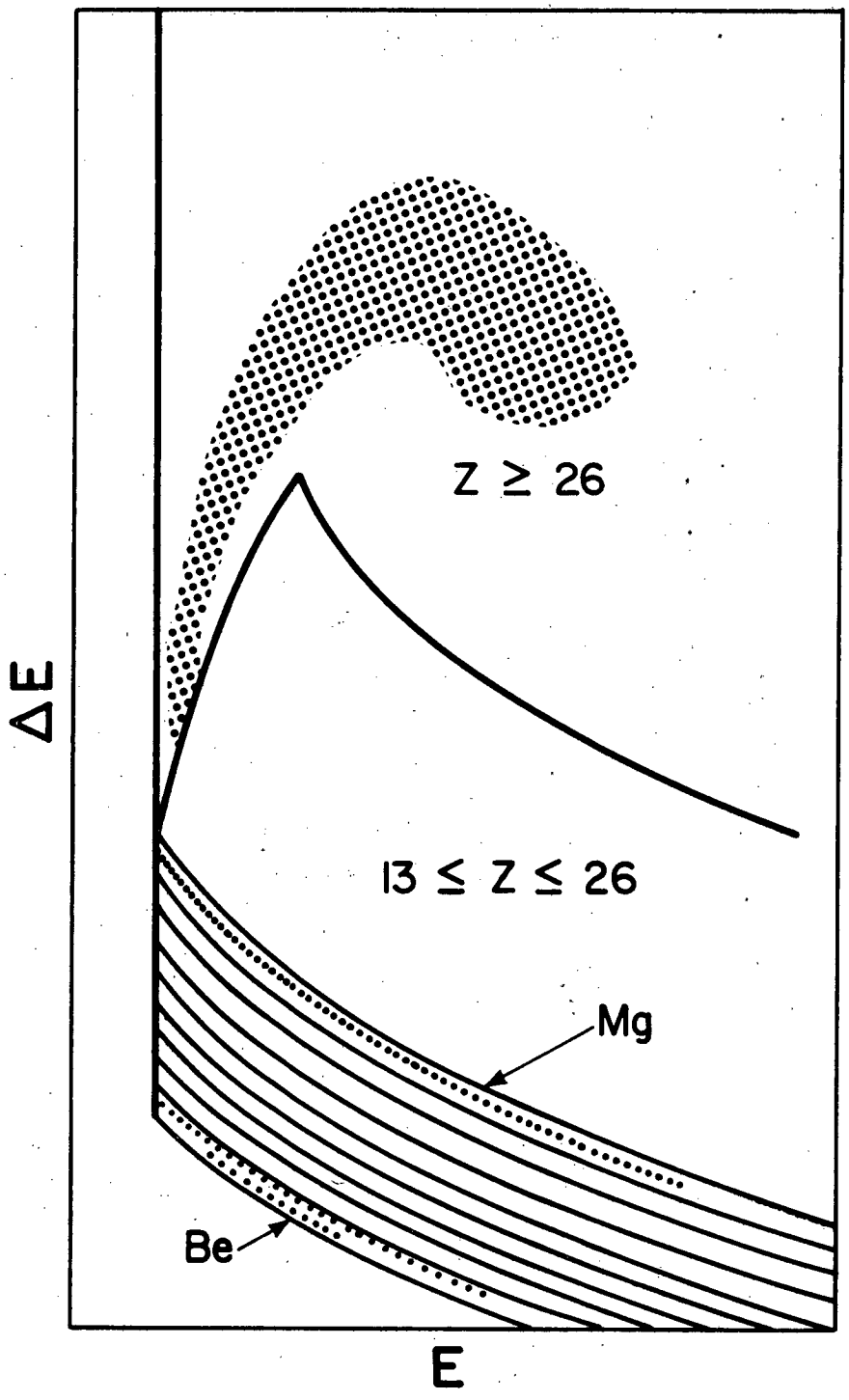

XBL 794-1096

Figure 3

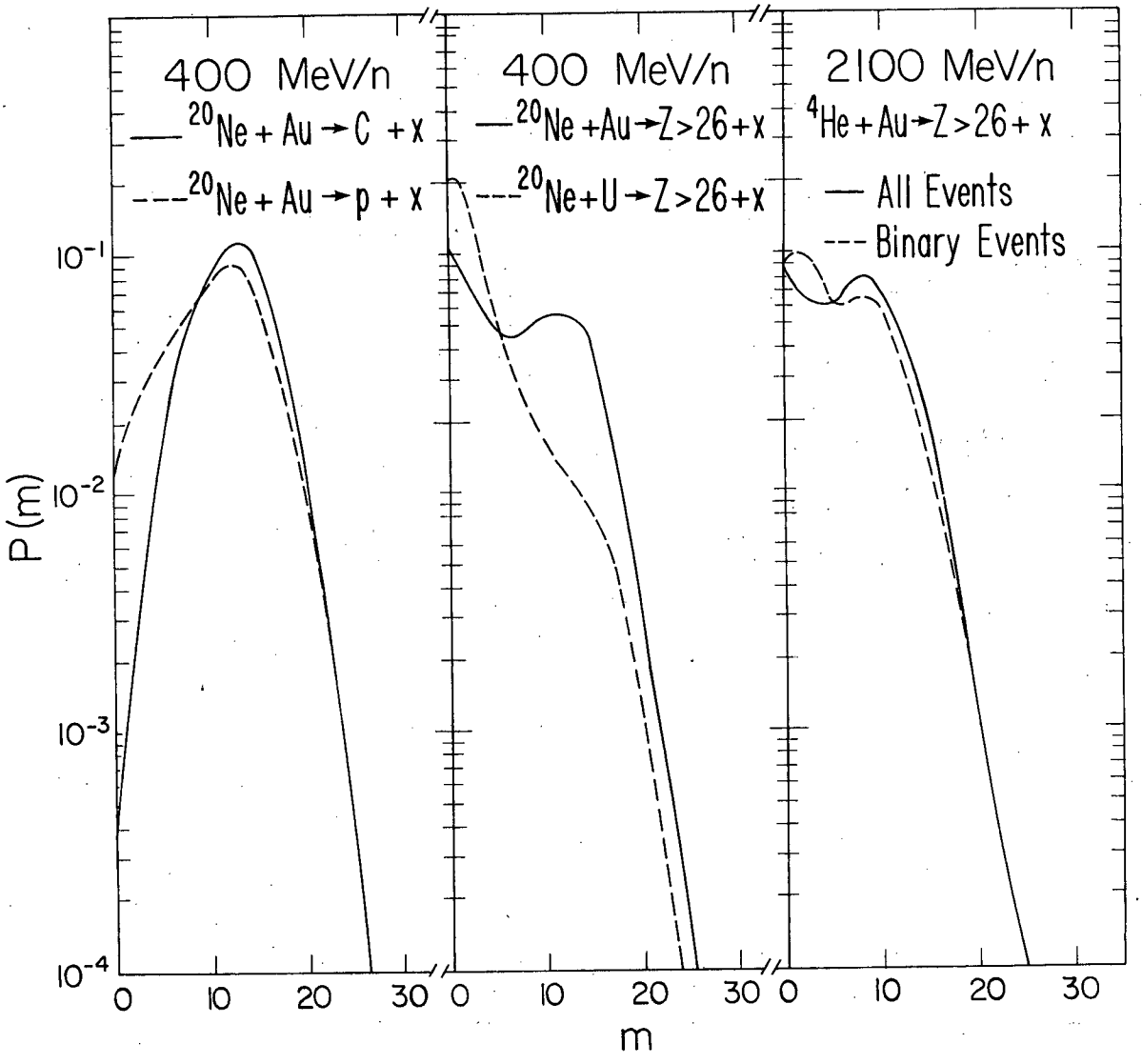

XBL 797-2140

Figure 4

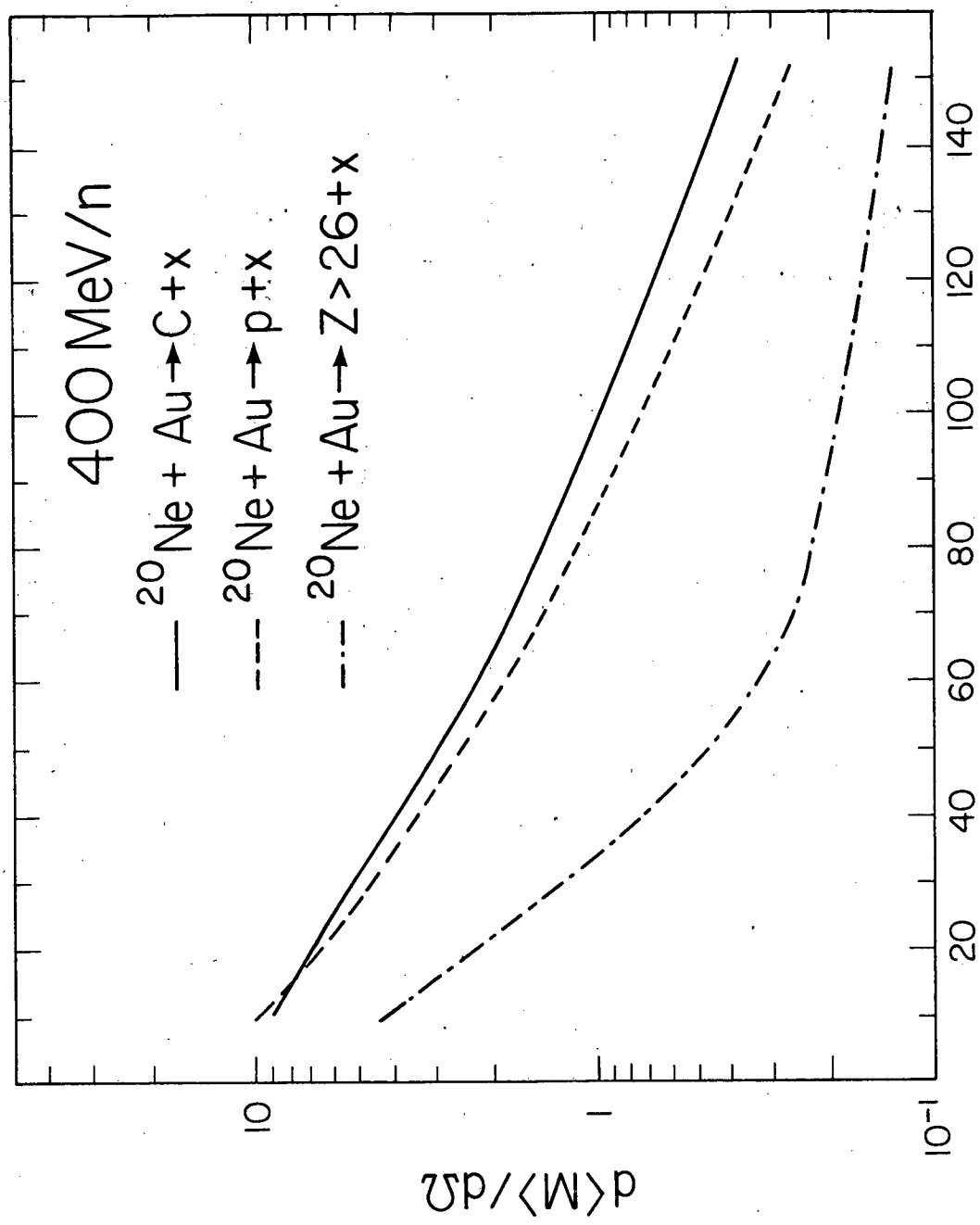

XBL 797-2139

Figure 5

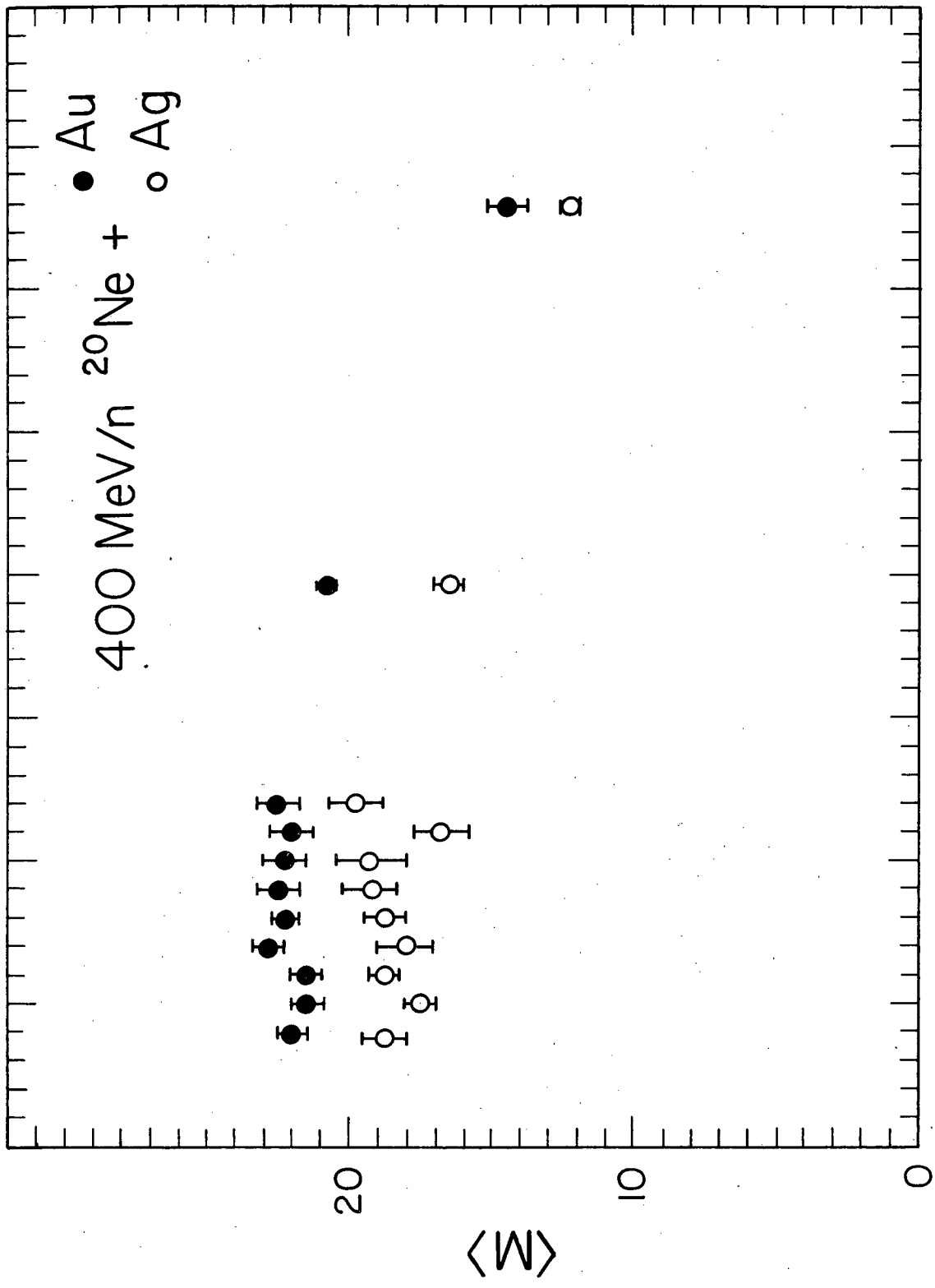

XBL 797-2136

Figure 6

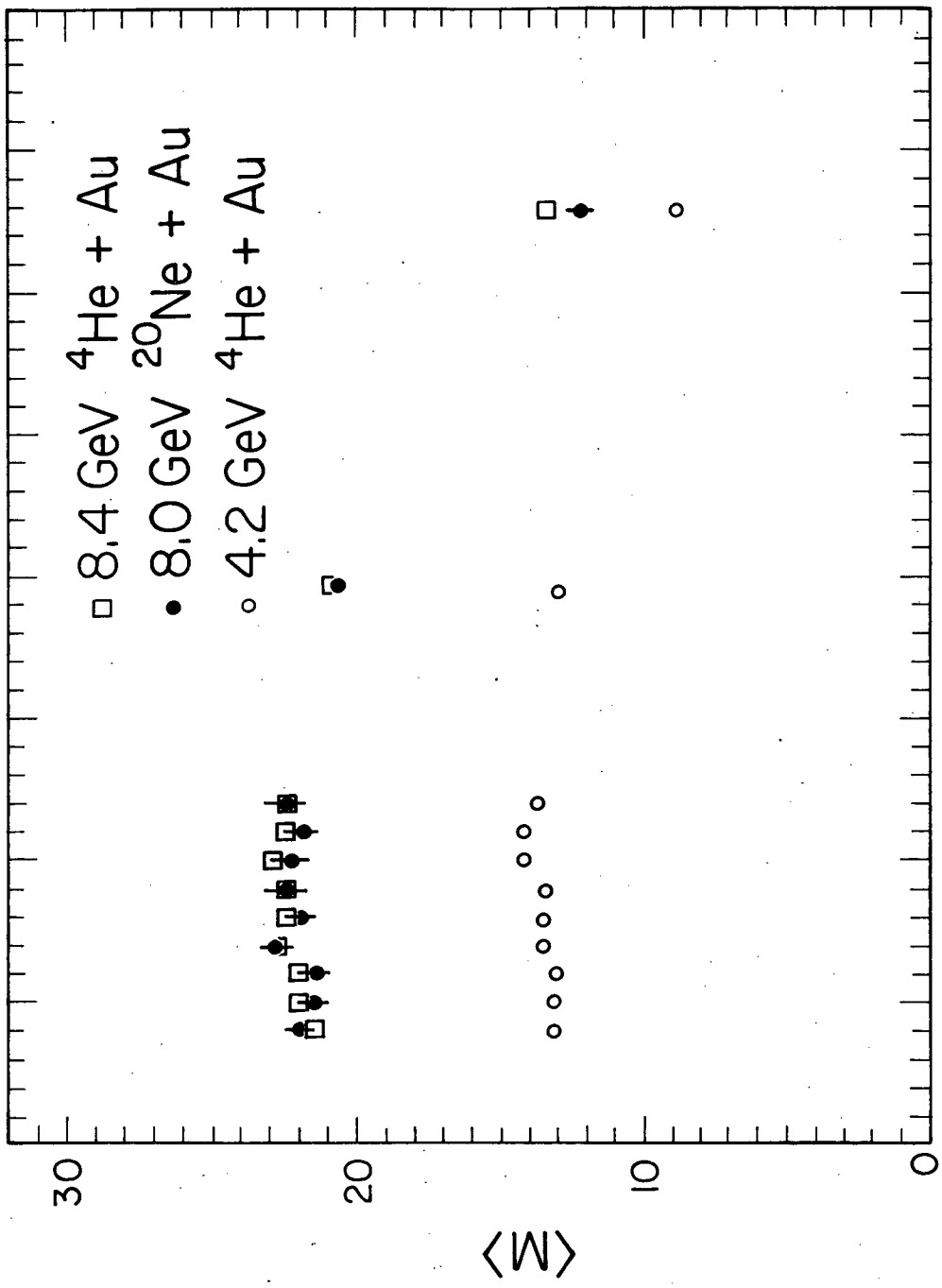

XBL 797-2135

Figure 7

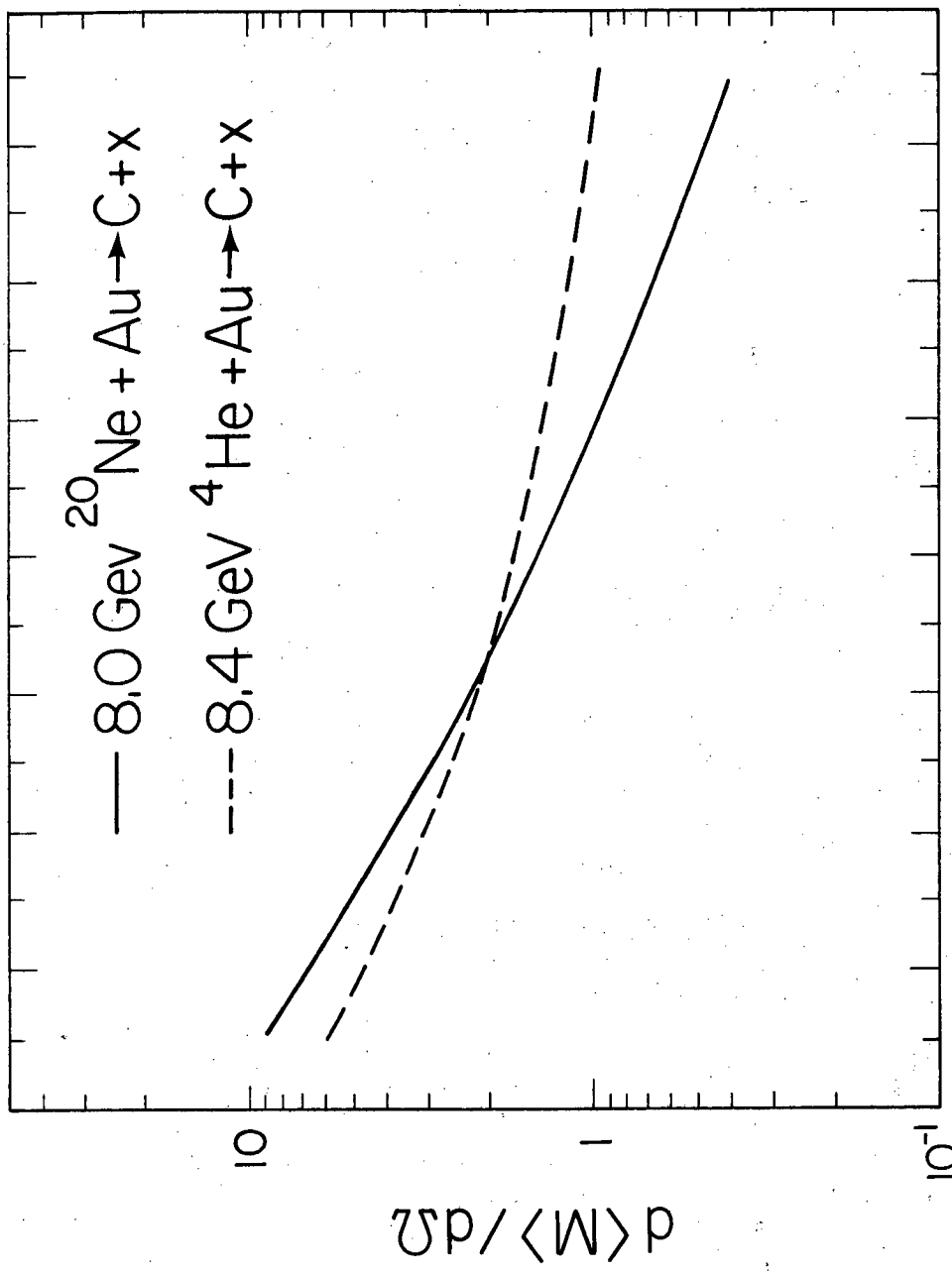

XBL 797-2138

Figure 8

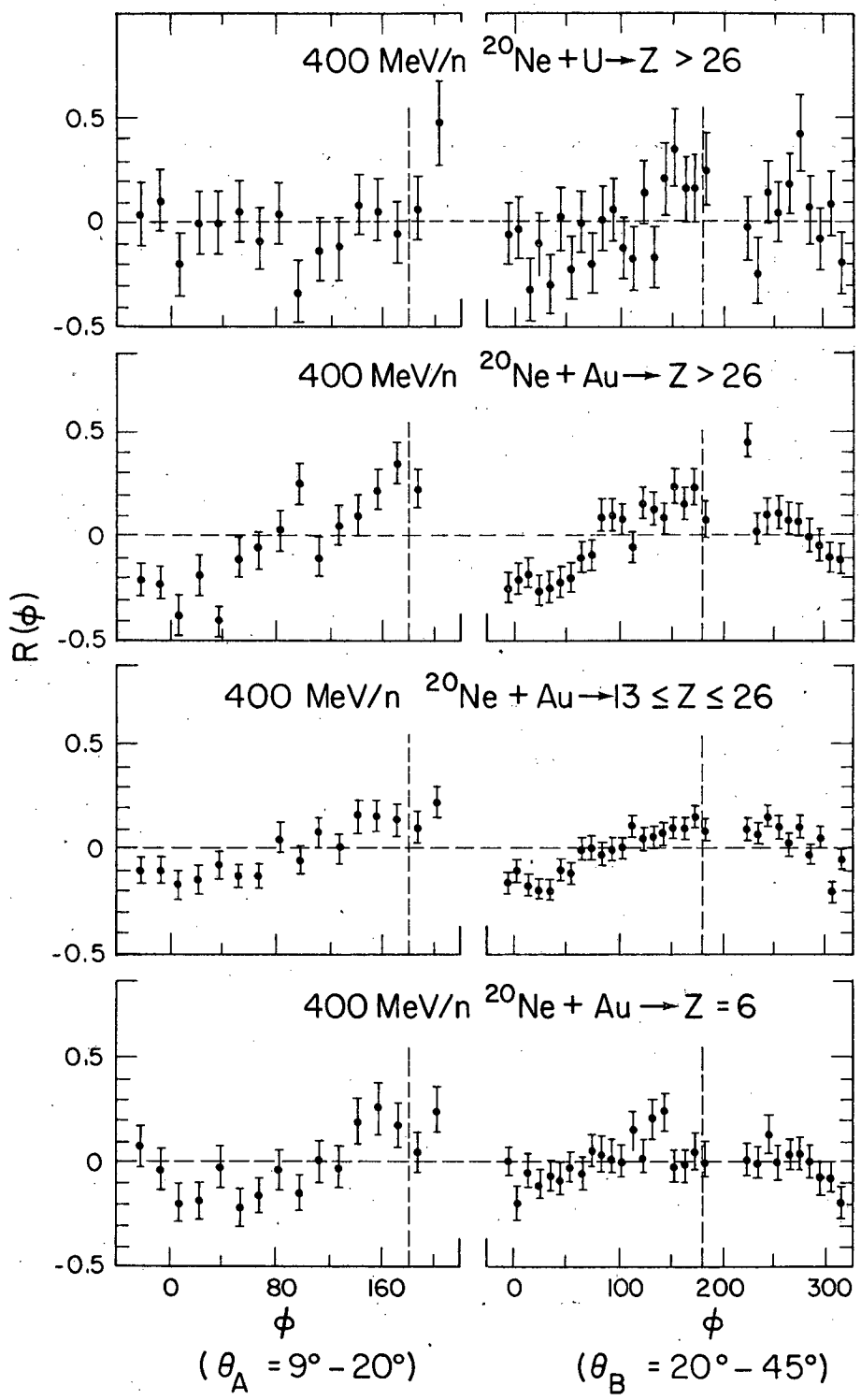

XBL 797-2210

Figure 9

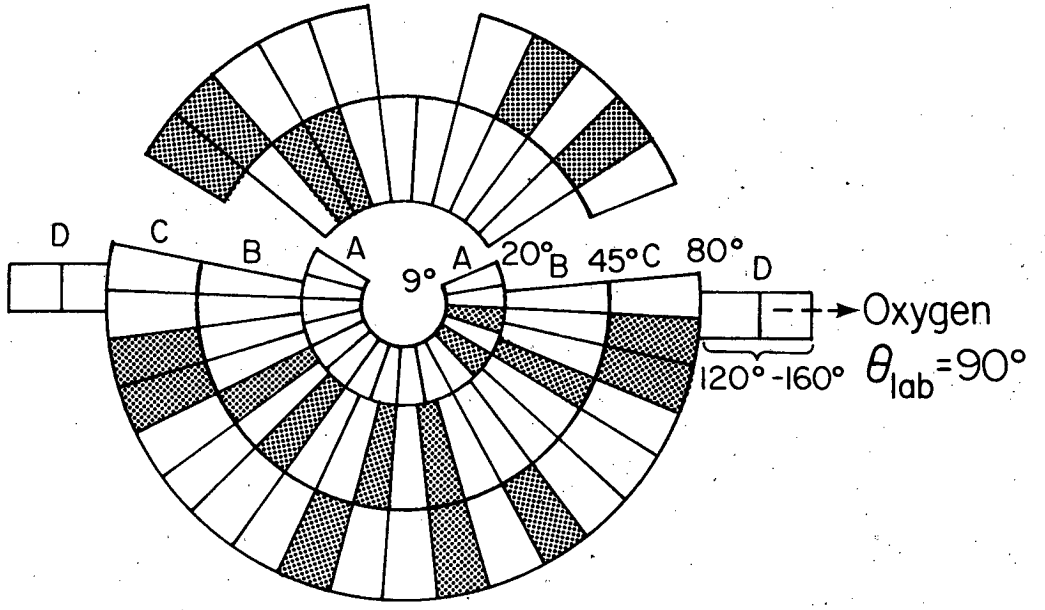

400 MeV/n ^{20}Ne + Au → Oxygen + x

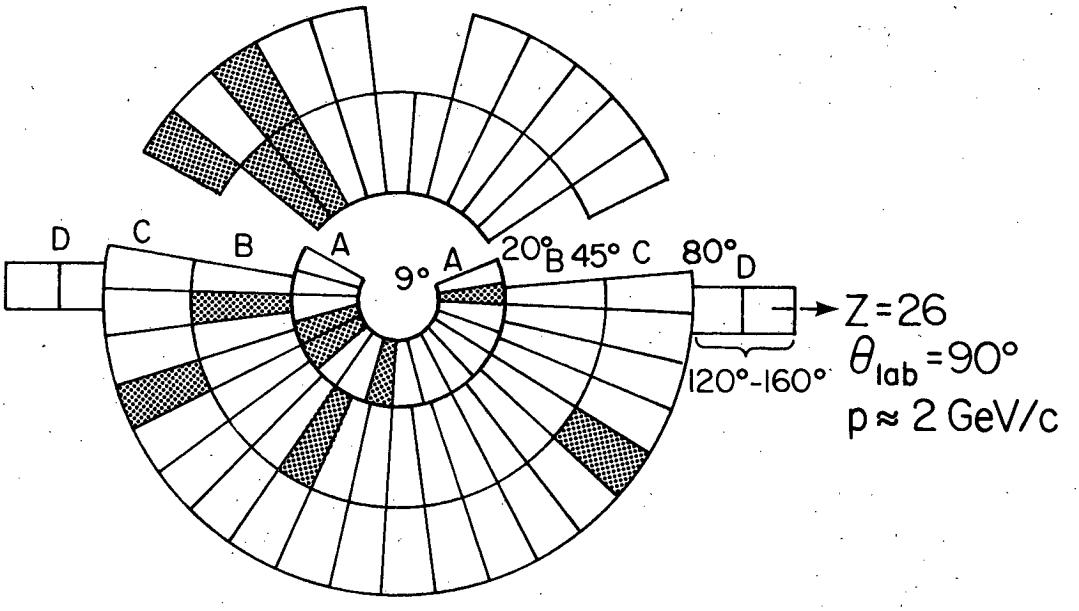

400 MeV/n ^{20}Ne + Ag → Z = 26 + x

XBL 797-2134

Figure 10

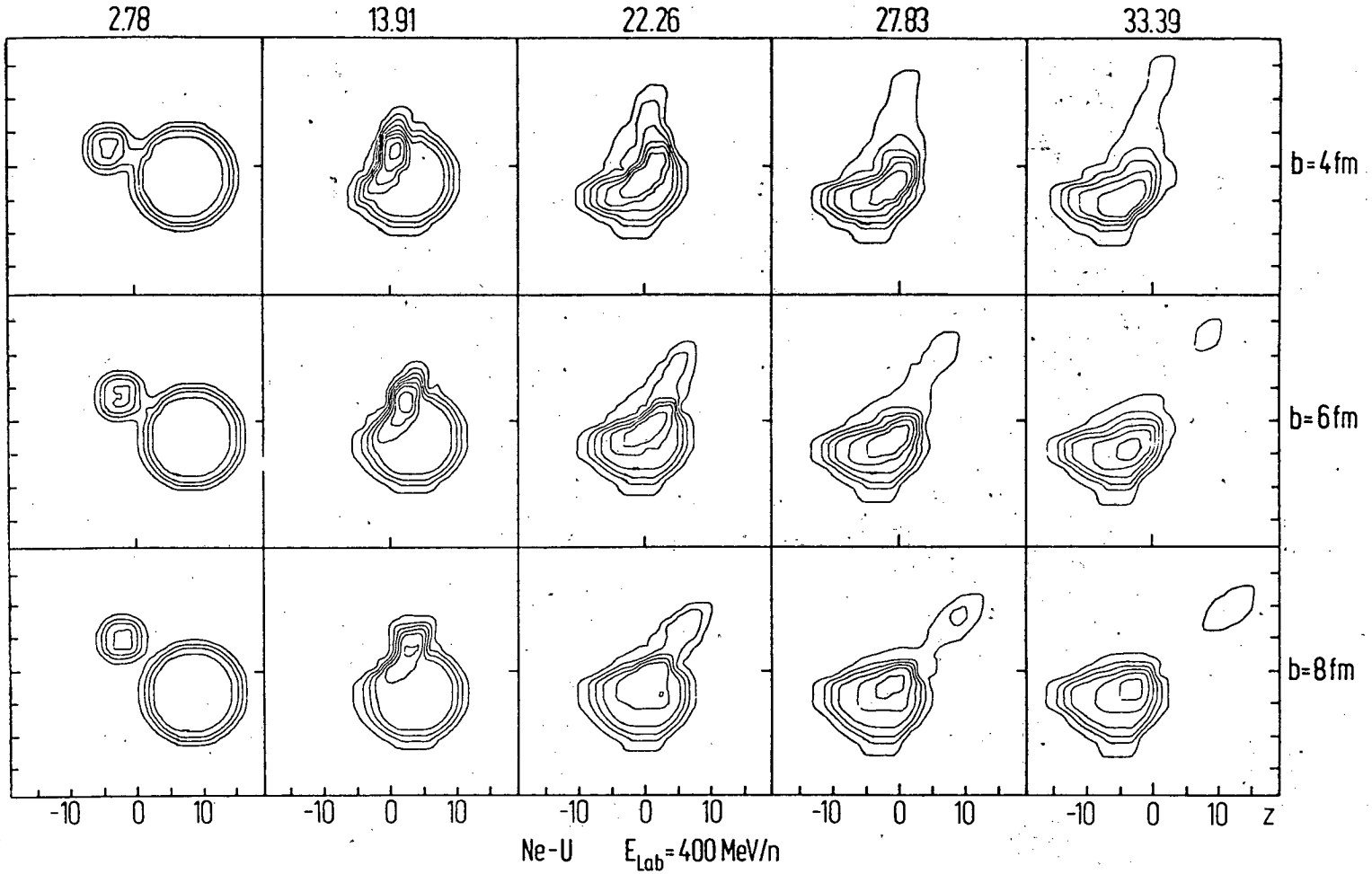
2.78
13.91
22.26
27.83
33.39
b=4fm
b=6fm
b=8fm
-10
0
10
z
Ne-U E_{Lab}=400 MeV/n
XBL 799-11758

Figure 11

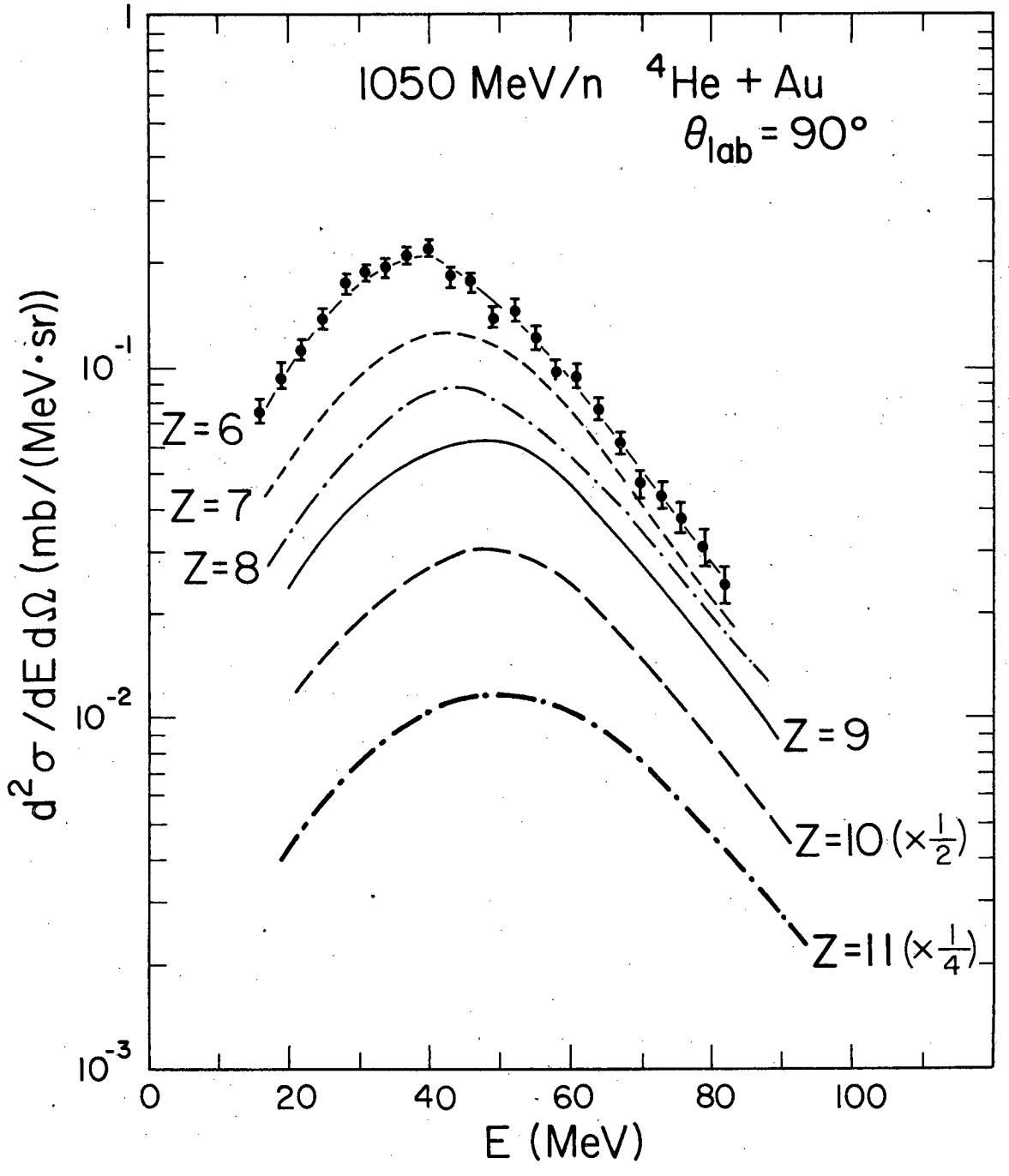

XBL 797-2209

Figure 12

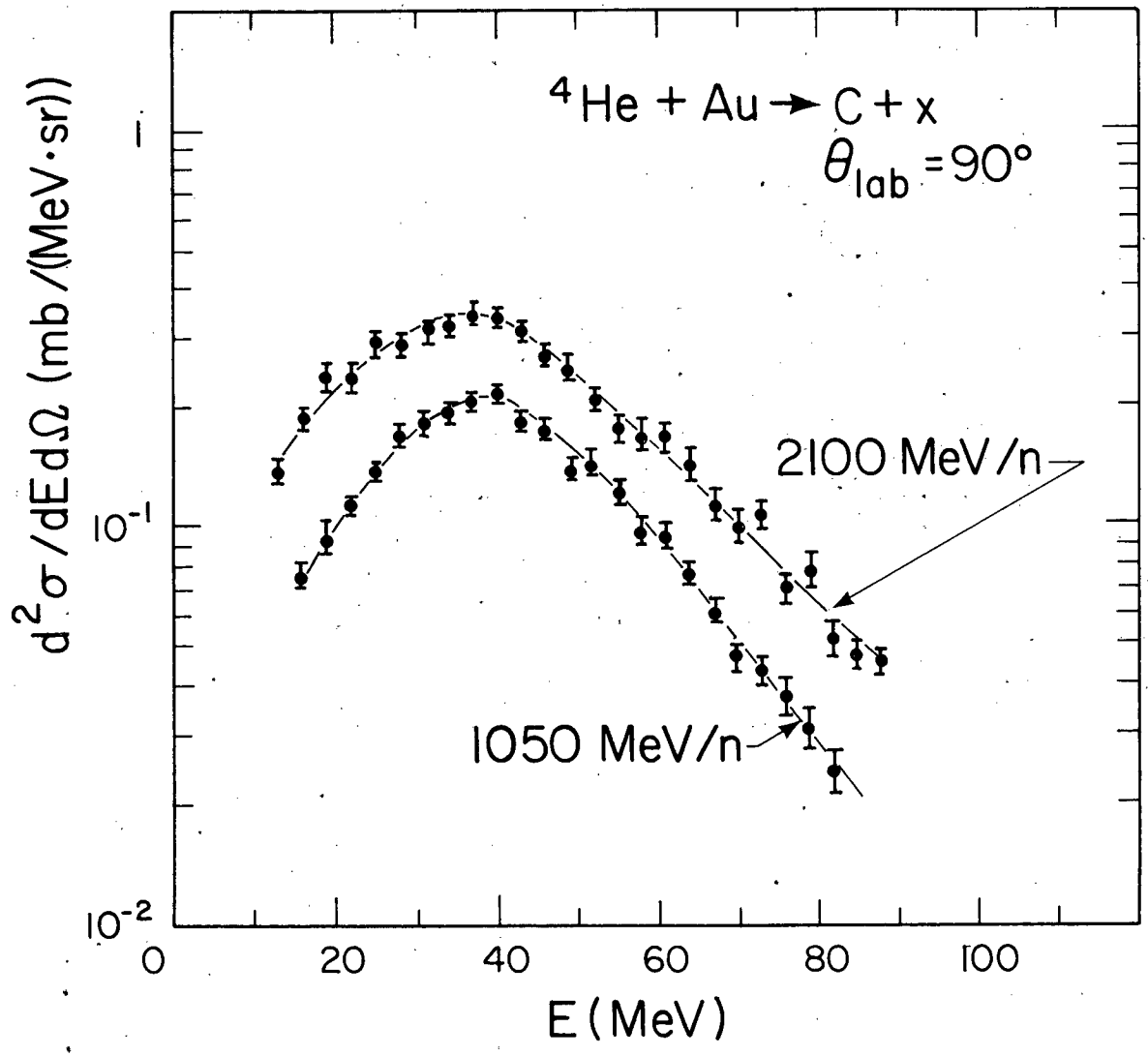

XBL 797-2208

Figure 13

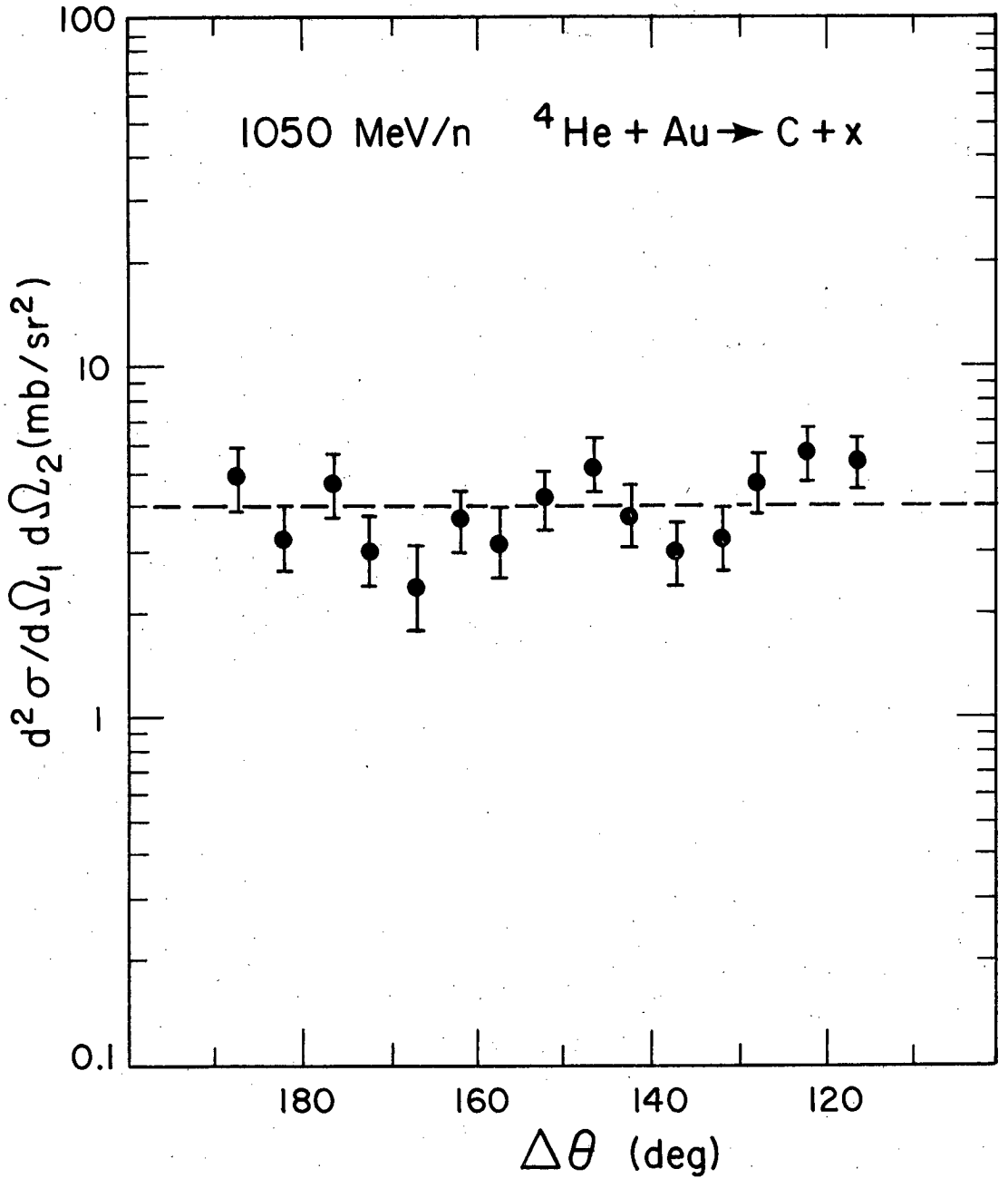

XBL 797-2238

Figure 14

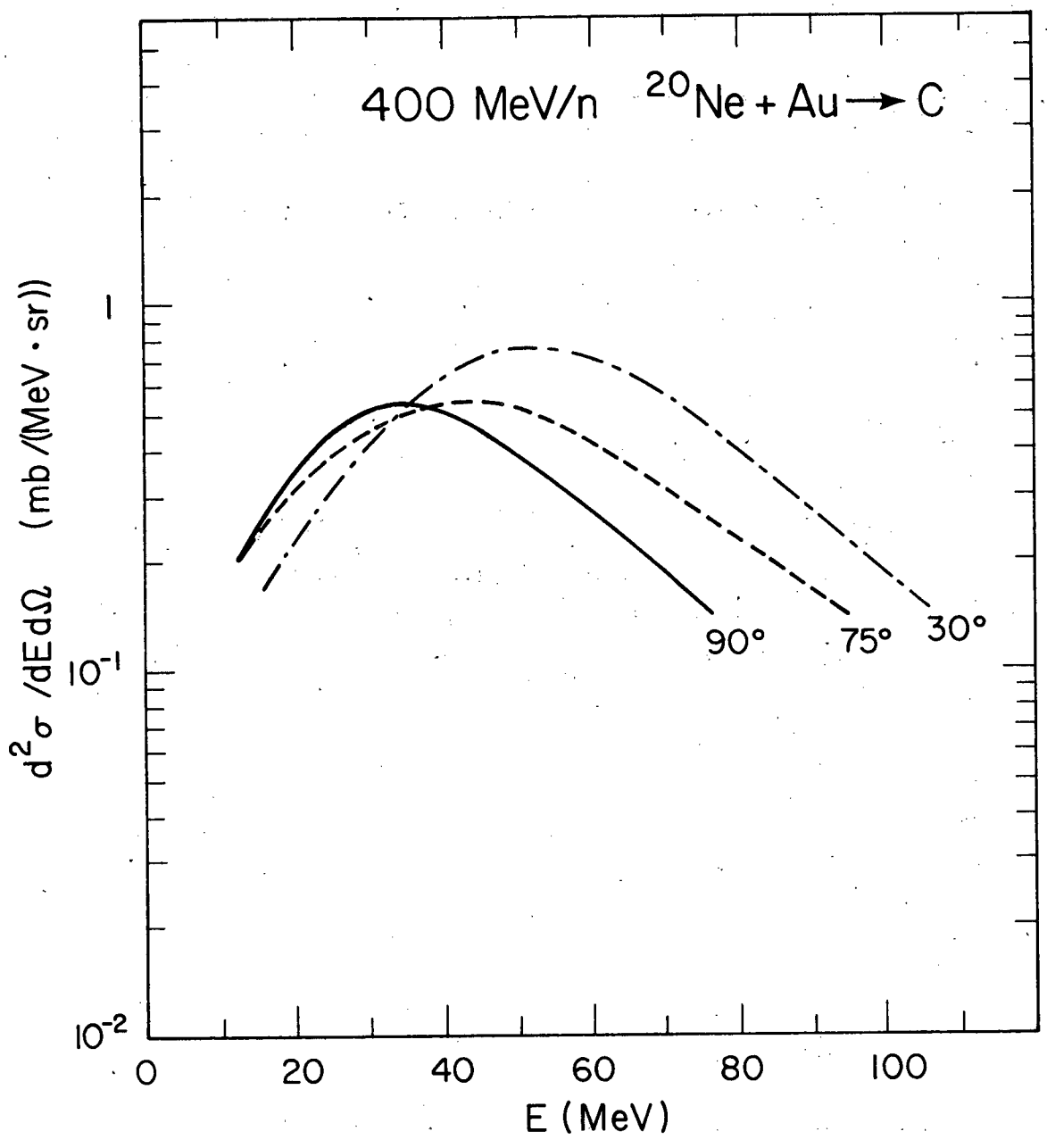

XBL 797-2137

Figure 15

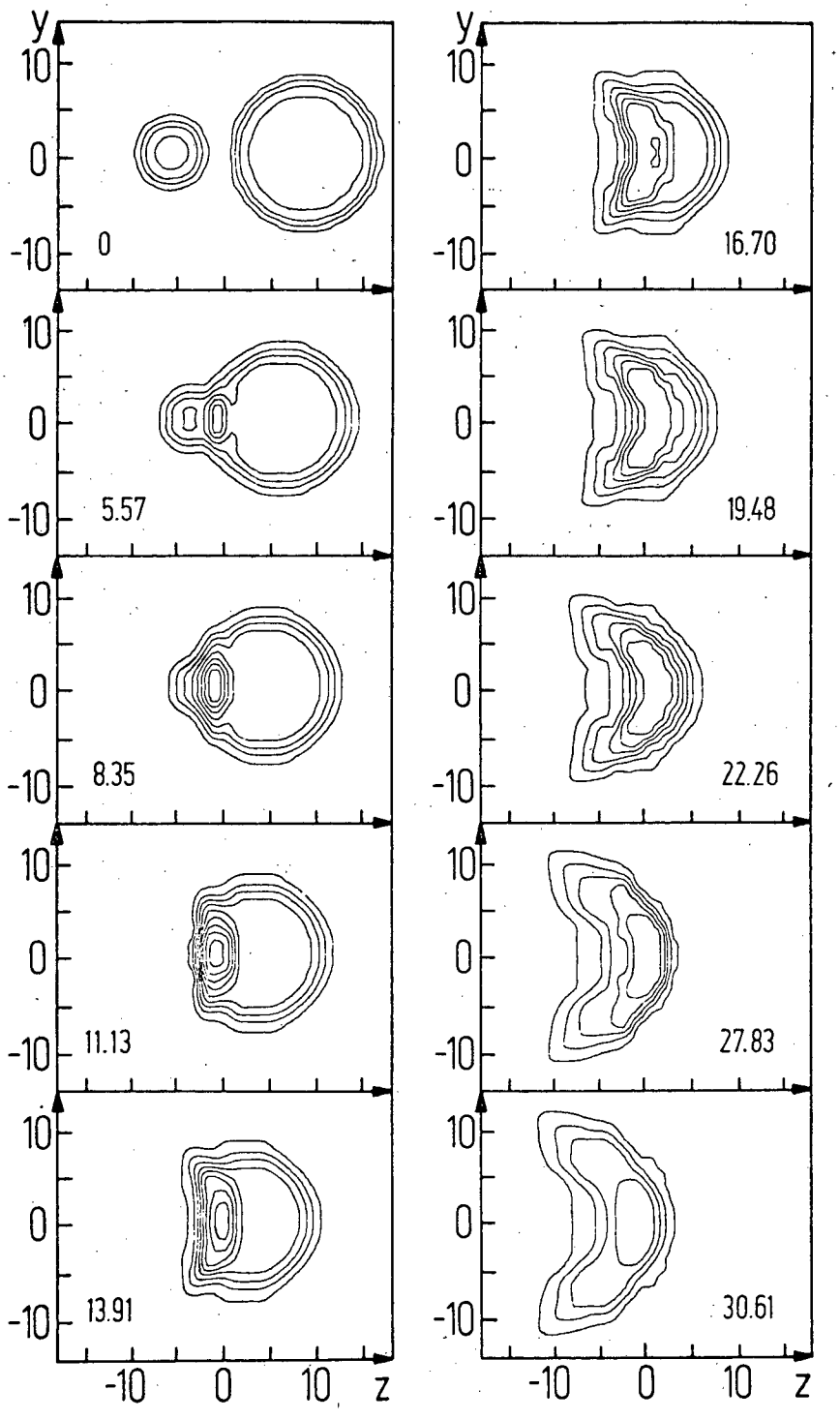

XBL 799-11757

Figure 16

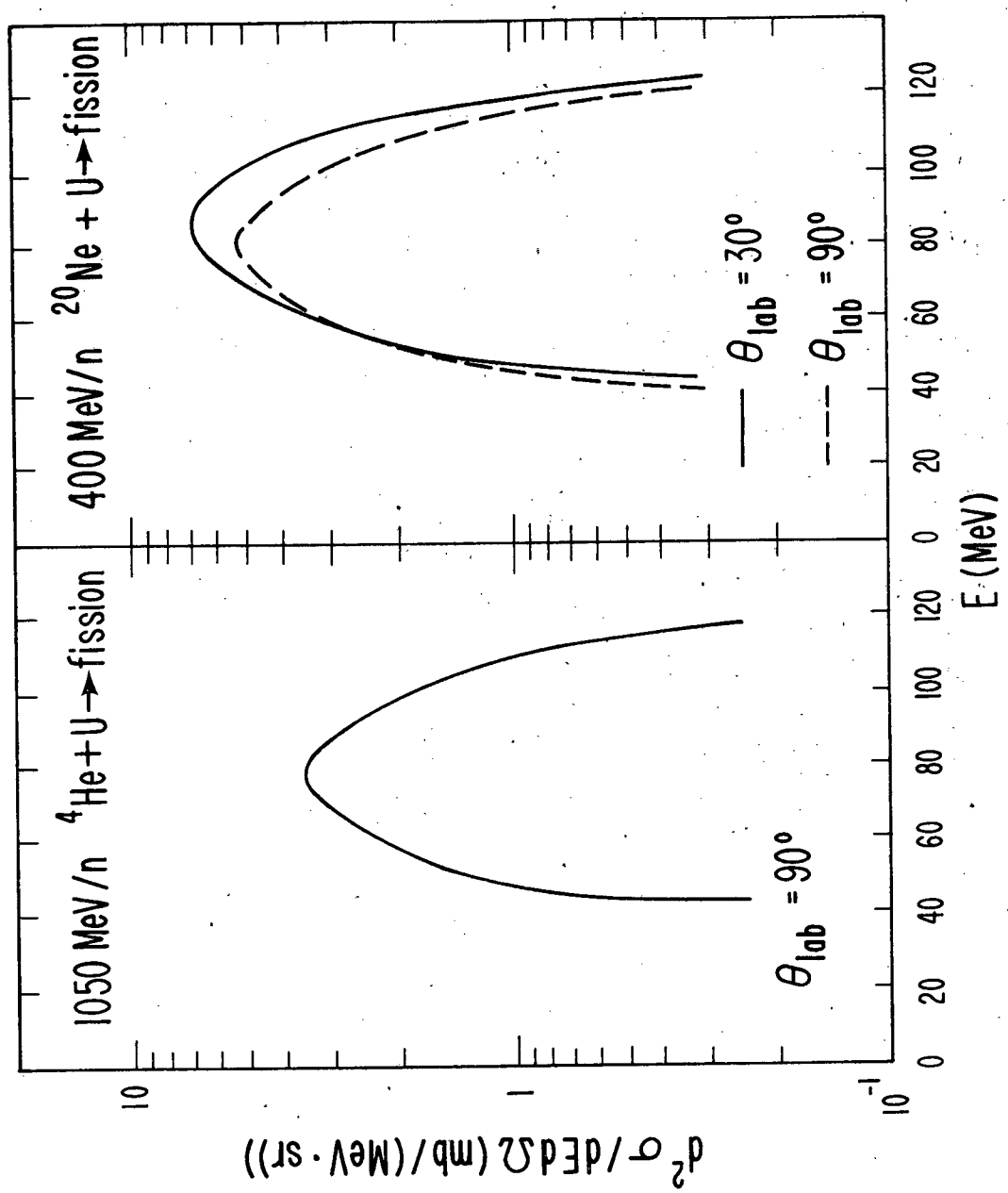

XBL 797-2239

Figure 17

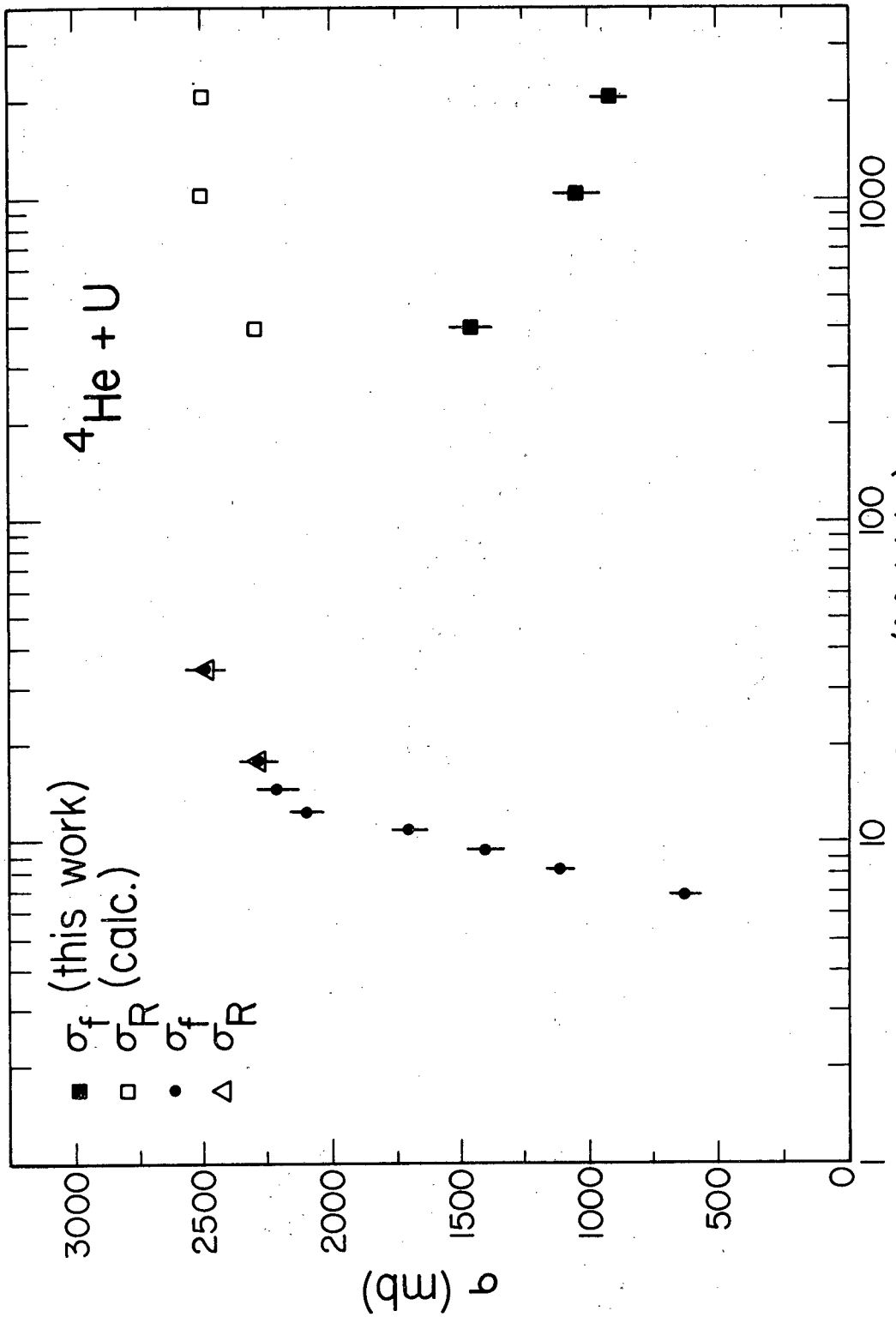
^{4}He + U
σ_f (this work)
σ_R (calc.)
σ_f
σ_R
σ (mb)
3000
2500
2000
1500
1000
500
0
10
100
1000
$E_{proj.}$ (MeV/n)
XBL 798-2513

Figure 18

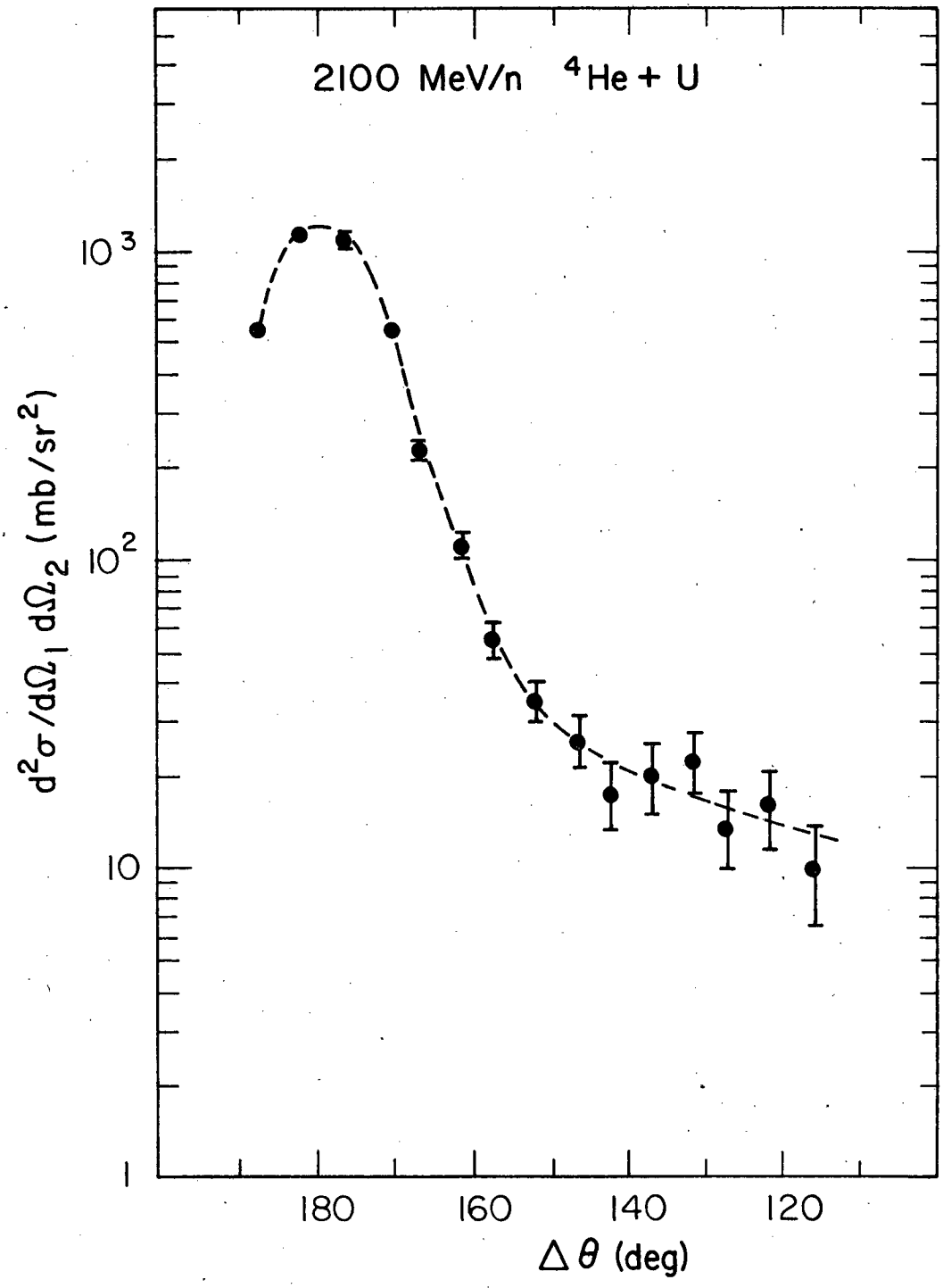

XBL 797-2240

Figure 19

TECHNICAL INFORMATION DEPARTMENT
LAWRENCE BERKELEY LABORATORY
UNIVERSITY OF CALIFORNIA
BERKELEY, CALIFORNIA 94720